Goal-oriented a posteriori error estimation for conforming and nonconforming approximations with inexact solvers

Gouranga Mallik, Martin Vohralík, Soleiman Yousef

Goal-oriented a posteriori error estimation for conforming and nonconforming approximations with inexact solvers*

Gouranga Mallik† Martin Vohralík‡§ Soleiman Yousef†

July 25, 2019

Abstract

We derive a unified framework for goal-oriented a posteriori estimation covering in particular higher-order conforming, nonconforming, and discontinuous Galerkin finite element methods, as well as the finite volume method. The considered problem is a model linear second-order elliptic equation with inhomogeneous Dirichlet and Neumann boundary conditions and the quantity of interest is given by an arbitrary functional composed of a volumetric weighted mean value (source) term and a surface weighted mean (Dirichlet boundary) flux term. We specifically do not request the primal and dual discrete problems to be resolved exactly, allowing for inexact solves. Our estimates are based on $\boldsymbol{H}(\mathrm{div})$-conforming flux reconstructions and H^1-conforming potential reconstructions and provide a guaranteed upper bound on the goal error. The overall estimator is split into components corresponding to the primal and dual discretization and algebraic errors, which are then used to prescribe efficient stopping criteria for the employed iterative algebraic solvers. Numerical experiments are performed for the finite volume method applied to the Darcy porous media flow problem in two and three space dimensions. They show excellent effectivity indices even in presence of primal and dual algebraic errors and enable to spare a large percentage of unnecessary algebraic iterations.

Key words: quantity of interest, a posteriori error estimate, guaranteed bound, inexact algebraic solver, equilibrated flux, unified framework, adaptivity.

1 Introduction

Goal-oriented *a posteriori error estimates* are a powerful tool in numerical approximations of many engineering problems since they provide relevant information about the error in a *quantity of interest* rather than about the error measured in some norm. The quantity of interest is expressed in terms of a functional $Q(\cdot)$. The technique of the estimates is based on the solution of an auxiliary (dual) problem, adjoint to the original (primal) problem.

The dual weighted residual (DWR) method promoted by Becker and Rannacher [5], see also [3, 7, 22, 24, 33], the general framework by Prodhumme and Oden [36, 40], the approach of Maday and Patera [31], multi-objective error estimation in [16, 23, 46], enhanced least-squares finite element

*This project has received funding from the European Research Council (ERC) under the European Unions Horizon 2020 research and innovation program (grant agreement No 647134 GATIPOR).

†IFP Energies nouvelles, 1 & 4 av. Bois Préau, 92852 Rueil-Malmaison, France (gouranga2011@gmail.com, soleiman.yousef@ifpen.fr).

‡Inria, 2 rue Simone Iff, 75589 Paris, France.

§Université Paris-Est, CERMICS (ENPC), 77455 Marne-la-Vallée, France (martin.vohralik@inria.fr).

methods by Chaudhry *et al.* [8], or the constitutive relation error (CRE) approach of Ladevèze *et al.* [28, 30] and Rey *et al.* [42–44], see also the references therein, are very popular approaches to goal-oriented error estimation; this can also be built in the discretization scheme as in Kergrene *et al.* [27]. The obtained bounds are, however, often not guaranteed in the sense of yielding a fully computable number that is rigorously greater than or equal to the goal error. Obtaining rigorous guaranteed bounds is possible upon introducing the equilibrated flux approach closely related to the CRE method. In particular, Ainsworth and Rankin [2] follow this path and develop and compare a number of alternative approaches, in the context of a linear second-order elliptic problem, also focusing on general inhomogeneous Dirichlet boundary conditions. Their idea is to split the error into two components where the first error is bounded by a computable dual-weighted residual and the second one, claimed small in [5], is estimated via equilibrated fluxes. An important focus whose rigorous investigation has been started only recently is the theory for nonconforming, discontinuous Galerkin, and mixed methods: let us cite in particular Mozolevski and Prudhomme [34] and Dolejší *et al.* [13, 15]. Finally, to the best of our knowledge, with the exception of [13, 32, 42–44], all the above-cited results rely on the assumption that both the primal and the dual discrete problems are *solved exactly*. This may not be satisfied in practical large-scale simulations and, actually, developing the theory not relying on such an assumption is a basis of *full adaptivity* including all meshes, polynomial degrees, and solvers, cf., e.g., [4, 18, 37] and the references therein.

The present article develops *a unified framework* for goal-oriented a posteriori error estimation for a model linear second-order elliptic equation. We consider inhomogeneous Dirichlet and Neumann boundary conditions and a goal functional including the "most demanding" (according to [3]) engineering application of the *normal flux* passing through some surface, unlike in most of the papers [24, 33, 34, 36, 40] which concern the primal variable evaluation around a region (point evaluation by regularization) or (point) evaluation of derivatives of the solution. We next apply this framework to various *finite element methods* (conforming, nonconforming, and discontinuous Galerkin) as well as to the *finite volume method*. We derive *guaranteed* goal-oriented a posteriori error estimates based on equilibrated flux and potential reconstruction, cf. [6, 10, 17, 20, 39] and the references therein, and treat the tricky "remainder" term in the goal error expression following [28, 29]. Our approach is significantly different from the well-known dual-weighted residual method [3, 5, 7, 22, 24, 33] and extends [34] upon also bounding essentially higher-order terms and including the case where the continuous and discrete solutions lead to the same goal $Q(u) = Q(u_h)$.

The discretization of the primal and dual problems yields two linear algebraic systems. We do not suppose here their exact resolution. This *inexact solution* of the linear systems influences the goal error as well as its estimates. Following the ideas of [4, 18, 25, 32, 37] and the references therein, we decompose the primal and dual estimates into estimates on discretization and algebraic error components. We can then prescribe efficient stopping criteria for iterative solvers applied to both primal and dual algebraic systems, balancing the two components.

This paper is organized as follows: Section 2 introduces setting and useful notation. Section 3 describes the model problem and the goal functional. Section 4 then establishes a posteriori error estimates for the goal functional in an abstract framework. In Section 5, we then show how to apply the framework to various discretization schemes. Finally, Section 6 proposes a fully adaptive algorithm with a posteriori stopping criteria for the primal and dual solvers and illustrates the theory by numerical experiments.

2 Setting

Let $\Omega \subset \mathbb{R}^d, d = 2, 3$ be a polygonal/polyhedral domain (open, bounded, and connected set) and denote by $\Gamma = \overline{\Gamma}_{\mathrm{D}} \cup \overline{\Gamma}_{\mathrm{N}}$ with $\Gamma_{\mathrm{D}} \cap \Gamma_{\mathrm{N}} = \emptyset$ the Lipschitz-continuous boundary $\partial\Omega$ of Ω. Throughout

the paper, standard notation of Lebesgue and Sobolev spaces is employed. We denote by $H^1_{u_\mathrm{D}}(\Omega)$ the subspace of $H^1(\Omega)$ of functions whose trace on the boundary Γ_D is a given function u_D, and for vanishing trace, we simply use the notation $H^1_\mathrm{D}(\Omega)$. The symbols ∇ and $\nabla\cdot$ are used respectively for the weak gradient and divergence. For a subdomain $\omega \subset \Omega$, we denote by $(\cdot,\cdot)_\omega$ the $L^2(\omega)$-inner product, by $\|\cdot\|_\omega$ the associated norm (we omit the index when $\omega = \Omega$), and by $|\omega|$ the Lebesgue measure of ω.

Let $\mathcal{T}_h$ be a conforming (matching) partition of $\overline{\Omega}$ into nonempty closed triangles or rectangles for $d = 2$ and tetrahedra or rectangular parallelepipeds for $d = 3$ such that $\overline{\Omega} = \cup_{K\in\mathcal{T}_h} K$ and such that the intersection of two different elements is either an empty set, a vertex, an edge, or a face. We call e an edge for $d = 2$ and face for $d = 3$ (in the sequel, we simply call e face). The faces of an element $K \in \mathcal{T}_h$ are collected in the set $\mathcal{E}_K$. We denote by $\mathcal{E}_h$ the set of all faces of $\mathcal{T}_h$, by $\mathcal{E}_h^\mathrm{int}$ the set of interior ones, and by $\mathcal{E}_h^\mathrm{ext}$ the set of boundary ones. Suppose that each boundary face lies entirely in $\overline{\Gamma}_\mathrm{D}$ or in $\overline{\Gamma}_\mathrm{N}$ and denote by $\mathcal{E}_h^\mathrm{D}$ the faces contained in $\overline{\Gamma}_\mathrm{D}$ and by $\mathcal{E}_h^\mathrm{N}$ those contained in $\overline{\Gamma}_\mathrm{N}$. A family of meshes $\{\mathcal{T}_h\}_h$ is parametrized by $h := \max_{K\in\mathcal{T}} h_K$, where h_K stands for the diameter of K; we also denote by h_e the diameter of $e \in \mathcal{E}_h$. Let $\mathcal{V}_h$ denote the set of mesh vertices with subsets $\mathcal{V}_h^\mathrm{int}$ for interior vertices and $\mathcal{V}_h^\mathrm{ext}$ for boundary ones. Let $\mathcal{V}_K$ denote the vertices of the element $K \in \mathcal{T}_h$, $\mathcal{V}_h^\mathrm{D}$ the set of boundary vertices lying in the closure of Γ_D, and $\mathcal{V}_h^\mathrm{N}$ the remaining boundary vertices. For each element $K \in \mathcal{T}_h$ and an each face $e \in \mathcal{E}_K$, we indicate by $\boldsymbol{n}_{K,e}$ the unit normal vector to e pointing outward from K. For a given partition $\mathcal{T}_h$ of Ω, let $H^1(\mathcal{T}_h) := \{\varphi \in L^2(\Omega); \varphi|_K \in H^1(K)\ \forall K \in \mathcal{T}_h\}$ be the broken Sobolev space. For $\varphi \in H^1(\mathcal{T})$, define the jump $[\![\varphi]\!]_e = \varphi|_K - \varphi|_L$ and the average $\{\!\{\varphi\}\!\}_e = \frac{1}{2}(\varphi|_K + \varphi|_L)$ across the interior face e of the adjacent elements K and L (the orientation is not important in what follows). Extend the definition of the jump and the average to face lying in boundary by $[\![\varphi]\!]_e = \varphi|_e$ and $\{\!\{\varphi\}\!\}_e = \varphi|_e$ for $e \in \mathcal{E}_h^\mathrm{ext}$. We omit the subscript e for jump and average if there is no confusion. For any vector-valued function, jump and average are understood component-wise.

We use $\mathbb{P}_p(K)$ (respectively, $\mathbb{Q}_p(K)$), $p \geq 0$, to denote polynomials in $K \in \mathcal{T}_h$ of total degree at most p (respectively, at most p in each variable), and $\mathbb{P}_p(\mathcal{T}_h)$ and $\mathbb{Q}_p(\mathcal{T}_h)$ to denote the corresponding broken scalar-valued piecewise polynomial spaces. Following the Raviart–Thomas space [41] on triangles and rectangles, and the Nédélec space [35] on tetrahedra and rectangular parallelepipeds if $d = 3$, cf. also [45], we also define the Raviart–Thomas–Nédélec finite element space associated with the partition $\mathcal{T}_h$ of the domain Ω. This contains vector-valued piecewise polynomials that are $\boldsymbol{H}(\mathrm{div}\,,\Omega)$-conforming, i.e., their normal trace is continuous, and take form

$$\boldsymbol{RTN}_p(\Omega) := \{\boldsymbol{v}_h \in \boldsymbol{H}(\mathrm{div}\,,\Omega) : \boldsymbol{v}_h|_K \in \boldsymbol{RTN}_p(K), \forall K \in \mathcal{T}_h\}, \tag{2.1}$$

where for triangular or tetrahedral partition $\boldsymbol{RTN}_p(K) := [\mathbb{P}_p(K)]^d + \boldsymbol{x}\mathbb{P}_p(K)$ and for rectangular or rectangular parallelepipeds partition $\boldsymbol{RTN}_p(K) := \mathbb{Q}_{p+1,p}(K) \times \mathbb{Q}_{p,p+1}(K)$ and $\boldsymbol{RTN}_p(K) := \mathbb{Q}_{p+1,p,p}(K) \times\mathbb{Q}_{p,p+1,p}(K) \times\mathbb{Q}_{p,p,p+1}(K)$ with $\mathbb{Q}_{.,.}(K)$ and $\mathbb{Q}_{.,.,.}(K)$ being the spaces of maximal polynomial degree separately for each variable.

3 Model problem

We consider the linear boundary-value diffusion problem of finding $u : \Omega \to \mathbb{R}$ such that

$$\begin{aligned} -\nabla\cdot(\underline{\boldsymbol{K}}\nabla u) &= f && \text{in } \Omega,\\ -\underline{\boldsymbol{K}}\nabla u\cdot\boldsymbol{n} &= \sigma_\mathrm{N} && \text{on } \Gamma_\mathrm{N},\\ u &= u_\mathrm{D} && \text{on } \Gamma_\mathrm{D}, \end{aligned} \tag{3.1}$$

where $\underline{\boldsymbol{K}}$ is a diffusion tensor, f is a source term, and σ_{N} and u_{D} prescribe the Neumann and Dirichlet boundary conditions, respectively. From the pressure head u, we define the Darcy velocity $\boldsymbol{\sigma} := -\underline{\boldsymbol{K}}\nabla u$. We also refer to u as *potential* and to $\boldsymbol{\sigma}$ as *flux*. We suppose that $\underline{\boldsymbol{K}}$ is symmetric, bounded, and uniformly positive definite. For simplicity, we assume that the data satisfy $\underline{\boldsymbol{K}} \in [\mathbb{P}_0(\mathcal{T}_h)]^{d\times d}$ (i.e. $\underline{\boldsymbol{K}}$ is piecewise constant on $\mathcal{T}_h$), $f \in \mathbb{P}_p(\mathcal{T}_h)$, $u_{\mathrm{D}} \in \mathbb{P}_p(\mathcal{E}_h^{\mathrm{D}}) \cap H^{\frac{1}{2}}(\Gamma_{\mathrm{D}})$, and $\sigma_{\mathrm{N}} \in \mathbb{P}_p(\mathcal{E}_h^{\mathrm{N}})$ on simplicial meshes, and similarly with $\mathbb{Q}_p$ in place of $\mathbb{P}_p$ on meshes consisting of rectangular parallelepipeds (i.e. the other data are piecewise p-degree polynomials). This avoids the introduction of data oscillation terms. With an abuse of notation, any continuous piecewise p-degree polynomial extension of u_{D} to $H^1_{u_{\mathrm{D}}}(\Omega)$ is also denoted by u_{D}.

The weak formulation of the problem (3.1) reads: find $u \in H^1_{u_{\mathrm{D}}}(\Omega)$ with $u = u_0 + u_{\mathrm{D}}$, $u_0 \in H^1_{\mathrm{D}}(\Omega)$, such that

$$(\underline{\boldsymbol{K}}\nabla u_0, \nabla v) = (f, v) - (\sigma_{\mathrm{N}}, v)_{\Gamma_{\mathrm{N}}} - (\underline{\boldsymbol{K}}\nabla u_{\mathrm{D}}, \nabla v) \quad \forall v \in H^1_{\mathrm{D}}(\Omega). \tag{3.2}$$

In this article, we are interested in the goal functional

$$Q(v) := \big(\tilde{f}, v\big) - \big(\underline{\boldsymbol{K}}\nabla v\cdot\boldsymbol{n}, \tilde{u}_{\mathrm{D}}\big)_{\Gamma_{\mathrm{D}}}, \quad v \in H^1(\mathcal{T}_h) \tag{3.3}$$

for some given weight functions (sometimes called extractors) $\tilde{f} \in \mathbb{P}_p(\mathcal{T}_h)$ and $\tilde{u}_{\mathrm{D}} \in \mathbb{P}_p(\mathcal{E}_h^{\mathrm{D}}) \cap H^{\frac{1}{2}}(\Gamma_{\mathrm{D}})$ (or with $\mathbb{Q}_p$ in place of $\mathbb{P}_p$). In (3.3), ∇ stands for the broken (elementwise) gradient $(\nabla v)|_K := \nabla(v|_K)$; we assume therein that $\underline{\boldsymbol{K}}\nabla v\cdot\boldsymbol{n} \in L^1(\Gamma_{\mathrm{D}})$ whenever $\tilde{u}_{\mathrm{D}} \neq 0$.: As above, any continuous piecewise p-degree polynomial extension of $\tilde{u}_{\mathrm{D}}$ to $H^1_{\tilde{u}_{\mathrm{D}}}(\Omega)$ is again denoted by $\tilde{u}_{\mathrm{D}}$ itself. We observe that the first term in (3.3) corresponds to the evaluation of the primal variable (pressure) which can be localized by an appropriate weight function $\tilde{f}$ (possibly only defined on the some mesh elements), and the second term corresponds to the normal flux passing through the boundary surface Γ_{D} with respect to the weight function $\tilde{u}_{\mathrm{D}}$. Note that the weight function $\tilde{u}_{\mathrm{D}}$ can be chosen as 1 on the surface Γ_{D} in order to have physical normal flux over Γ_{D}, or localized on just some faces from $\mathcal{E}_h^{\mathrm{D}}$. We analyze the above goal functional with the help of the dual problem (note that $\underline{\boldsymbol{K}}$ is symmetric) to (3.1) which consists in finding $\tilde{u} : \Omega \to \mathbb{R}$ such that

$$\begin{aligned} -\nabla\cdot(\underline{\boldsymbol{K}}\nabla\tilde{u}) &= \tilde{f} && \text{in } \Omega,\\ -\underline{\boldsymbol{K}}\nabla\tilde{u}\cdot\boldsymbol{n} &= 0 && \text{on } \Gamma_{\mathrm{N}},\\ \tilde{u} &= \tilde{u}_{\mathrm{D}} && \text{on } \Gamma_{\mathrm{D}}, \end{aligned} \tag{3.4}$$

and its weak formulation seeks $\tilde{u} \in H^1_{\tilde{u}_{\mathrm{D}}}(\Omega)$ with $\tilde{u} = \tilde{u}_0 + \tilde{u}_{\mathrm{D}}$, $\tilde{u}_0 \in H^1_{\mathrm{D}}(\Omega)$, such that

$$(\underline{\boldsymbol{K}}\nabla\tilde{u}_0, \nabla v) = (\tilde{f}, v) - (\underline{\boldsymbol{K}}\nabla\tilde{u}_{\mathrm{D}}, \nabla v) \quad \forall v \in H^1_{\mathrm{D}}(\Omega). \tag{3.5}$$

Existence and uniqueness of the weak solutions of both the primal and dual problems (3.2) and (3.5) classically follow from Riesz representation theorem. Below, we often use the energy norm: for $\boldsymbol{v} \in [L^2(\omega)]^d$,

$$\|\boldsymbol{v}\|_{\underline{\boldsymbol{K}}^{-\frac{1}{2}};\omega} := \left\{\int_\omega \left|\underline{\boldsymbol{K}}^{-\frac{1}{2}}(\boldsymbol{x})\boldsymbol{v}(\boldsymbol{x})\right|^2 \,\mathrm{d}\boldsymbol{x}\right\}^{\frac{1}{2}}.$$

If $\omega = \Omega$, we simply denote the above norm by $\|\cdot\|_{\underline{\boldsymbol{K}}^{-\frac{1}{2}}}$.

4 Goal-oriented error estimate

In this section we derive an abstract a posteriori estimate on the error in the goal functional. Let respectively u_h^i and $\tilde{u}_h^i$ be arbitrary piecewise polynomial functions in $\mathbb{P}_p(\mathcal{T}_h)$ or $\mathbb{Q}_p(\mathcal{T}_h)$, with $(u_h^i, 1) = 0$ and $(\tilde{u}_h^i, 1) = 0$ for the pure Neumann case $\Gamma_{\rm N} = \Gamma$; the developments of this section hold for non-piecewise-polynomials but we stick to this for clarity. The index i will later denote the algebraic solver iteration.

4.1 Potential and flux reconstructions and the Prager–Synge equality

We start with some basic definitions and results.

Definition 4.1 (Potential reconstruction)**.** *We call a potential reconstruction any piecewise polynomial scalar-valued function s_h^i (resp. $\tilde{s}_h^i$) locally constructed from u_h^i (resp. $\tilde{u}_h^i$) which satisfies*

$$s_h^i \in H^1(\Omega) \cap \mathbb{P}_p(\mathcal{T}_h) \text{ or } \mathbb{Q}_p(\mathcal{T}_h) \quad (\text{resp. } \tilde{s}_h^i \in H^1(\Omega) \cap \mathbb{P}_p(\mathcal{T}_h) \text{ or } \mathbb{Q}_p(\mathcal{T}_h)), \tag{4.1a}$$

$$(s_h^i, 1) = 0 \quad (\text{resp. } (\tilde{s}_h^i, 1) = 0) \qquad \text{when } \Gamma_{\rm N} = \Gamma, \tag{4.1b}$$

$$s_h^i|_{\Gamma_{\rm D}} = u_{\rm D} \quad (\text{resp. } \tilde{s}_h^i|_{\Gamma_{\rm D}} = \tilde{u}_{\rm D}) \qquad \text{when } \Gamma_{\rm D} \neq 0. \tag{4.1c}$$

Note that one can write $s_h^i = s_{h,0}^i + u_{\rm D}$ with $s_{h,0}^i \in H^1_{\rm D}(\Omega) \cap \mathbb{P}_p(\mathcal{T}_h)$ or $\mathbb{Q}_p(\mathcal{T}_h)$ and similarly for $\tilde{s}_h^i$.

Definition 4.2 (Equilibrated flux reconstruction)**.** *We call an equilibrated flux reconstruction any piecewise polynomial vector-valued function $\boldsymbol{\sigma}_h^i$ (resp. $\tilde{\boldsymbol{\sigma}}_h^i$) locally constructed from u_h^i (resp. $\tilde{u}_h^i$) which satisfies*

$$\boldsymbol{\sigma}_h^i \in \boldsymbol{RTN}_p(\Omega) \quad (\text{resp. } \tilde{\boldsymbol{\sigma}}_h^i \in \boldsymbol{RTN}_p(\Omega)), \tag{4.2a}$$

$$\nabla\cdot\boldsymbol{\sigma}_h^i = f \quad (\text{resp. } \nabla\cdot\tilde{\boldsymbol{\sigma}}_h^i = \tilde{f}) \qquad \text{in } \Omega, \tag{4.2b}$$

$$\boldsymbol{\sigma}_h^i\cdot\boldsymbol{n} = \sigma_{\rm N} \quad (\text{resp. } \tilde{\boldsymbol{\sigma}}_h^i\cdot\boldsymbol{n} = 0) \qquad \text{on } \Gamma_{\rm N} \qquad \text{when } \Gamma_{\rm N} \neq \emptyset. \tag{4.2c}$$

The classical result of Prager and Synge [39] implies:

Corollary 4.3 (Prager–Synge equality for the primal problem)**.** *Let $u \in H^1_{u_{\rm D}}(\Omega)$ be the solution of (3.2) and let $s_h^i \in H^1_{u_{\rm D}}(\Omega)$ be an arbitrary potential reconstruction following Definition 4.1. Let $\boldsymbol{\sigma}_h^i \in \boldsymbol{H}(\mathrm{div}, \Omega)$ be an arbitrary equilibrated flux reconstruction of Definition 4.2. Then*

$$\|\underline{\boldsymbol{K}}\nabla(u - s_h^i)\|^2_{\underline{\boldsymbol{K}}^{-\frac{1}{2}}} + \|\underline{\boldsymbol{K}}\nabla u + \boldsymbol{\sigma}_h^i\|^2_{\underline{\boldsymbol{K}}^{-\frac{1}{2}}} = \|\underline{\boldsymbol{K}}\nabla s_h^i + \boldsymbol{\sigma}_h^i\|^2_{\underline{\boldsymbol{K}}^{-\frac{1}{2}}}. \tag{4.3}$$

A similar result to Corollary 4.3 holds for dual problem:

Corollary 4.4 (Prager–Synge equality for the dual problem)**.** *Let $\tilde{u} \in H^1_{\tilde{u}_{\rm D}}(\Omega)$ be the solution of (3.5) and $\tilde{s}_h^i \in H^1_{\tilde{u}_{\rm D}}(\Omega)$ be an arbitrary potential reconstruction following Definition 4.1. Let $\tilde{\boldsymbol{\sigma}}_h^i \in \boldsymbol{H}(\mathrm{div}, \Omega)$ be an arbitrary equilibrated flux reconstruction of Definition 4.2. Then*

$$\|\underline{\boldsymbol{K}}\nabla(\tilde{u} - \tilde{s}_h^i)\|^2_{\underline{\boldsymbol{K}}^{-\frac{1}{2}}} + \|\underline{\boldsymbol{K}}\nabla\tilde{u} + \tilde{\boldsymbol{\sigma}}_h^i\|^2_{\underline{\boldsymbol{K}}^{-\frac{1}{2}}} = \|\underline{\boldsymbol{K}}\nabla\tilde{s}_h^i + \tilde{\boldsymbol{\sigma}}_h^i\|^2_{\underline{\boldsymbol{K}}^{-\frac{1}{2}}}. \tag{4.4}$$

4.2 Equivalent form of the goal functional

We now turn to the goal functional Q of (3.3). We start by the following equality:

Theorem 4.5 (Goal error equation)**.** *Let u and $\tilde{u}$ be respectively the solutions of (3.2) and (3.5). Let u_h^i and $\tilde{u}_h^i \in \mathbb{P}_p(\mathcal{T}_h)$ or $\mathbb{Q}_p(\mathcal{T}_h)$ be arbitrary discontinuous piecewise polynomial functions. Let s_h^i and $\tilde{s}_h^i$ be the potential reconstructions of Definition 4.1, and $\boldsymbol{\sigma}_h^i$ and $\tilde{\boldsymbol{\sigma}}_h^i$ be the equilibrated flux reconstructions of Definition 4.2. Then there holds*

$$Q(u) - Q(u_h^i) = -\left(\underline{\boldsymbol{K}}\nabla s_h^i + \boldsymbol{\sigma}_h^i, \nabla\tilde{u}\right) + \left((\underline{\boldsymbol{K}}\nabla s_h^i + \boldsymbol{\sigma}_h^i)\cdot\boldsymbol{n}, \tilde{u}_{\mathrm{D}}\right)_{\Gamma_{\mathrm{D}}} + Q(s_h^i - u_h^i). \tag{4.5}$$

Proof. Using (3.2) together with $\tilde{u}|_{\Gamma_{\mathrm{D}}} = \tilde{u}_{\mathrm{D}}$ and $(-\underline{\boldsymbol{K}}\nabla u\cdot\boldsymbol{n}, \tilde{u})_{\Gamma_{\mathrm{N}}} = (\sigma_{\mathrm{N}}, \tilde{u})_{\Gamma_{\mathrm{N}}}$ and by applying integration by parts, one can write

$$(\underline{\boldsymbol{K}}\nabla u, \nabla\tilde{u}) = -(\nabla\cdot(\underline{\boldsymbol{K}}\nabla u), \tilde{u}) + (\underline{\boldsymbol{K}}\nabla u\cdot\boldsymbol{n}, \tilde{u})_{\partial\Omega} = (f, \tilde{u}) + (\underline{\boldsymbol{K}}\nabla u\cdot\boldsymbol{n}, \tilde{u}_{\mathrm{D}})_{\Gamma_{\mathrm{D}}} - (\sigma_{\mathrm{N}}, \tilde{u})_{\Gamma_{\mathrm{N}}}.$$

Next, using the decomposition $u = u_0 + u_{\mathrm{D}}$, the weak formulation (3.5) with test function $v = u_0$, and the symmetry of $\underline{\boldsymbol{K}}$, the same left-hand side term can be written as

$$(\underline{\boldsymbol{K}}\nabla u, \nabla\tilde{u}) = (\underline{\boldsymbol{K}}\nabla u_0, \nabla\tilde{u}) + (\underline{\boldsymbol{K}}\nabla u_{\mathrm{D}}, \nabla\tilde{u}) = (\tilde{f}, u_0) + (\underline{\boldsymbol{K}}\nabla u_{\mathrm{D}}, \nabla\tilde{u}).$$

Recall the goal functional (3.3) applied to u:

$$Q(u) = (\tilde{f}, u) - (\underline{\boldsymbol{K}}\nabla u\cdot\boldsymbol{n}, \tilde{u}_{\mathrm{D}})_{\Gamma_{\mathrm{D}}}. \tag{4.6}$$

Combining the above two equations, we obtain the representation of the normal flux term from the goal functional $Q(u)$ as

$$(\underline{\boldsymbol{K}}\nabla u\cdot\boldsymbol{n}, \tilde{u}_{\mathrm{D}})_{\Gamma_{\mathrm{D}}} = (\tilde{f}, u_0) + (\underline{\boldsymbol{K}}\nabla u_{\mathrm{D}}, \nabla\tilde{u}) - (f, \tilde{u}) + (\sigma_{\mathrm{N}}, \tilde{u})_{\Gamma_{\mathrm{N}}}. \tag{4.7}$$

With the normal flux identity (4.7), the goal functional (4.6) can be written as

$$Q(u) = (\tilde{f}, u_{\mathrm{D}}) - (\underline{\boldsymbol{K}}\nabla u_{\mathrm{D}}, \nabla\tilde{u}) + (f, \tilde{u}) - (\sigma_{\mathrm{N}}, \tilde{u})_{\Gamma_{\mathrm{N}}}. \tag{4.8}$$

Definition 4.2 of the equilibrated flux $\boldsymbol{\sigma}_h^i$ further yields, also employing that $\tilde{u}$ on Γ_{D} equals $\tilde{u}_{\mathrm{D}}$,

$$Q(u) = (\tilde{f}, u_{\mathrm{D}}) - (\underline{\boldsymbol{K}}\nabla u_{\mathrm{D}}, \nabla\tilde{u}) - (\boldsymbol{\sigma}_h^i, \nabla\tilde{u}) + (\boldsymbol{\sigma}_h^i\cdot\boldsymbol{n}, \tilde{u}_{\mathrm{D}})_{\Gamma_{\mathrm{D}}}. \tag{4.9}$$

The identity of the goal functional (4.9) and the definition of $Q(s_h^i)$ then lead to the goal error in the potential s_h^i

$$Q(u) - Q(s_h^i) = -(\tilde{f}, s_{h,0}^i) - (\underline{\boldsymbol{K}}\nabla u_{\mathrm{D}}, \nabla\tilde{u}) - (\boldsymbol{\sigma}_h^i, \nabla\tilde{u}) + \left((\underline{\boldsymbol{K}}\nabla s_h^i + \boldsymbol{\sigma}_h^i)\cdot\boldsymbol{n}, \tilde{u}_{\mathrm{D}}\right)_{\Gamma_{\mathrm{D}}},$$

while using that $s_h^i = s_{h,0}^i + u_{\mathrm{D}}$. Adding and subtracting $Q(u_h^i)$ implies

$$Q(u) - Q(u_h^i) = -(\tilde{f}, s_{h,0}^i) - (\underline{\boldsymbol{K}}\nabla u_{\mathrm{D}}, \nabla\tilde{u}) - (\boldsymbol{\sigma}_h^i, \nabla\tilde{u}) + \left((\underline{\boldsymbol{K}}\nabla s_h^i + \boldsymbol{\sigma}_h^i)\cdot\boldsymbol{n}, \tilde{u}_{\mathrm{D}}\right)_{\Gamma_{\mathrm{D}}} + Q(s_h^i - u_h^i). \tag{4.10}$$

Observe that here, the first and the last terms only depend on available discrete quantities, and in the two middle terms, the first arguments are also known. Now, by choosing the test function $v = s_{h,0}^i \in H^1_{\mathrm{D}}(\Omega)\cap\mathbb{P}_p(\mathcal{T}_h)$ or $\mathbb{Q}_p(\mathcal{T}_h)$ in the weak formulation (3.5) and using the symmetry of $\underline{\boldsymbol{K}}$, we infer that

$$(\tilde{f}, s_{h,0}^i) + (\underline{\boldsymbol{K}}\nabla u_{\mathrm{D}}, \nabla\tilde{u}) = (\underline{\boldsymbol{K}}\nabla\tilde{u}, \nabla s_{h,0}^i) + (\underline{\boldsymbol{K}}\nabla\tilde{u}, \nabla u_{\mathrm{D}}) = (\underline{\boldsymbol{K}}\nabla\tilde{u}, \nabla s_h^i). \tag{4.11}$$

Finally, by combining the above expressions (4.10) and (4.11) with the symmetry of $\underline{\boldsymbol{K}}$, we obtain the final goal error expression (4.5). □

Remark 4.6 (Comparison with [34, Theorem 1]). *For the case of a goal functional without normal flux, i.e.* $\tilde{u}_{\mathrm{D}} = 0$, *Mozolevski and Prudhomme in [34, Theorem 1] propose the error representation with respect to a discontinuous finite element approximation* $u_h^i \in \mathbb{P}_p(\mathcal{T}_h)$ *as*

$$\begin{aligned} Q(u) - Q(u_h^i) = (\underline{\boldsymbol{K}}\nabla u_h^i + \boldsymbol{\sigma}_h^i, \underline{\boldsymbol{K}}^{-1}\tilde{\boldsymbol{\sigma}}_h^i) - \sum_{e\in\mathcal{E}_h} \left([\![u_h^i]\!], \tilde{\boldsymbol{\sigma}}_h^i\cdot\boldsymbol{n}_e\right)_e \\ - (\underline{\boldsymbol{K}}\nabla u_h^i + \boldsymbol{\sigma}_h^i, \nabla\tilde{u} + \underline{\boldsymbol{K}}^{-1}\tilde{\boldsymbol{\sigma}}_h^i) + \sum_{e\in\mathcal{E}_h} \left([\![u_h^i]\!], (\underline{\boldsymbol{K}}\nabla\tilde{u} + \tilde{\boldsymbol{\sigma}}_h^i)\cdot\boldsymbol{n}_e\right)_e, \end{aligned} \tag{4.12}$$

where the first two terms provide asymptotic a posteriori estimator for the goal error in view of the higher order convergence rate of the last two terms which are disregarded. Moreover, the article excludes the case $Q(u) = Q(u_h^i)$ *in which the asymptotic estimator may overestimate the error.*

4.3 A posteriori error estimate of the goal functional

We now present our abstract framework for the estimation of the error in the goal functional. We start by the following simple estimate based on Theorem 4.5 and Corollary 4.4:

Remark 4.7 (Simple estimate). *Adding and subtracting* $(\underline{\boldsymbol{K}}\nabla s_h^i + \boldsymbol{\sigma}_h^i, \nabla\tilde{s}_h^i)$ *in the right-hand side of* (4.5) *yields*

$$\begin{aligned} Q(u) - Q(u_h^i) = &-(\underline{\boldsymbol{K}}\nabla s_h^i + \boldsymbol{\sigma}_h^i, \nabla(\tilde{u} - \tilde{s}_h^i)) - (\underline{\boldsymbol{K}}\nabla s_h^i + \boldsymbol{\sigma}_h^i, \nabla\tilde{s}_h^i) \\ &+ \left((\underline{\boldsymbol{K}}\nabla s_h^i + \boldsymbol{\sigma}_h^i)\cdot\boldsymbol{n}, \tilde{u}_{\mathrm{D}}\right)_{\Gamma_{\mathrm{D}}} + Q(s_h^i - u_h^i). \end{aligned} \tag{4.13}$$

Corollary 4.4 yields $\|\underline{\boldsymbol{K}}\nabla(\tilde{u} - \tilde{s}_h^i)\|_{\underline{\boldsymbol{K}}^{-\frac{1}{2}}} \le \|\underline{\boldsymbol{K}}\nabla\tilde{s}_h^i + \tilde{\boldsymbol{\sigma}}_h^i\|_{\underline{\boldsymbol{K}}^{-\frac{1}{2}}}$. *This and the Cauchy–Schwarz inequality lead to an a posteriori error estimate of* (4.13) *as*

$$\begin{aligned} |Q(u) - Q(u_h^i)| \le \|\underline{\boldsymbol{K}}\nabla s_h^i + \boldsymbol{\sigma}_h^i\|_{\underline{\boldsymbol{K}}^{-\frac{1}{2}}} \|\underline{\boldsymbol{K}}\nabla\tilde{s}_h^i + \tilde{\boldsymbol{\sigma}}_h^i\|_{\underline{\boldsymbol{K}}^{-\frac{1}{2}}} \\ + \left|-(\underline{\boldsymbol{K}}\nabla s_h^i + \boldsymbol{\sigma}_h^i, \nabla\tilde{s}_h^i) + \left((\underline{\boldsymbol{K}}\nabla s_h^i + \boldsymbol{\sigma}_h^i)\cdot\boldsymbol{n}, \tilde{u}_{\mathrm{D}}\right)_{\Gamma_{\mathrm{D}}} + Q(s_h^i - u_h^i)\right|. \end{aligned} \tag{4.14}$$

Estimate (4.14) may turn out quite precise in many cases but it has been observed by Ladevèze *et al.* [28–30] for the linear elasticity problem that it can overestimate the error. We thus modify the simple a posteriori estimate (4.14) following Ladevèze *et al.* [28–30]. Let

$$\tilde{\boldsymbol{\sigma}}_h^{i,\mathrm{m}} := \frac{1}{2}\left(\tilde{\boldsymbol{\sigma}}_h^i - \underline{\boldsymbol{K}}\nabla\tilde{s}_h^i\right) \tag{4.15}$$

be the average of the dual flux reconstruction of Definition 4.2 and of the gradient of the dual potential reconstruction of Definition 4.1. Adding and subtracting $(\underline{\boldsymbol{K}}\nabla s_h^i + \boldsymbol{\sigma}_h^i, \underline{\boldsymbol{K}}^{-1}\tilde{\boldsymbol{\sigma}}_h^{i,\mathrm{m}})$ in (4.5) leads to:

Theorem 4.8 (Abstract a posteriori estimate). *Let* u *and* $\tilde{u}$ *be respectively the solutions of* (3.2) *and* (3.5). *Let* u_h^i *and* $\tilde{u}_h^i \in \mathbb{P}_p(\mathcal{T}_h)$ *or* $\mathbb{Q}_p(\mathcal{T}_h)$ *be respectively arbitrary discontinuous piecewise polynomial functions. Let* s_h^i *and* $\tilde{s}_h^i$ *be the potential reconstructions of Definition 4.1, and* $\boldsymbol{\sigma}_h^i$ *and* $\tilde{\boldsymbol{\sigma}}_h^i$ *be the equilibrated flux reconstructions of Definition 4.2. Let finally* $\tilde{\boldsymbol{\sigma}}_h^{i,\mathrm{m}}$ *be the average flux reconstruction of* (4.15). *Then, there holds*

$$\begin{aligned} &\left|Q(u) - Q(u_h^i) - \left(\underline{\boldsymbol{K}}\nabla s_h^i + \boldsymbol{\sigma}_h^i, \underline{\boldsymbol{K}}^{-1}\tilde{\boldsymbol{\sigma}}_h^{i,\mathrm{m}}\right)\right| \\ &\le \frac{1}{2}\|\underline{\boldsymbol{K}}\nabla s_h^i + \boldsymbol{\sigma}_h^i\|_{\underline{\boldsymbol{K}}^{-\frac{1}{2}}} \|\underline{\boldsymbol{K}}\nabla\tilde{s}_h^i + \tilde{\boldsymbol{\sigma}}_h^i\|_{\underline{\boldsymbol{K}}^{-\frac{1}{2}}} + \left|\left((\underline{\boldsymbol{K}}\nabla s_h^i + \boldsymbol{\sigma}_h^i)\cdot\boldsymbol{n}, \tilde{u}_{\mathrm{D}}\right)_{\Gamma_{\mathrm{D}}} + Q(s_h^i - u_h^i)\right|. \end{aligned} \tag{4.16}$$

Proof. Adding and subtracting $(\underline{\boldsymbol{K}}\nabla s_h^i + \boldsymbol{\sigma}_h^i, \underline{\boldsymbol{K}}^{-1}\tilde{\boldsymbol{\sigma}}_h^{i,\mathrm{m}})$ in the right-hand side of the error representation (4.5) yields

$$\begin{aligned} Q(u) - Q(u_h^i) = & -\left(\underline{\boldsymbol{K}}\nabla s_h^i + \boldsymbol{\sigma}_h^i, \nabla\tilde{u} + \underline{\boldsymbol{K}}^{-1}\tilde{\boldsymbol{\sigma}}_h^{i,\mathrm{m}}\right) + \left(\underline{\boldsymbol{K}}\nabla s_h^i + \boldsymbol{\sigma}_h^i, \underline{\boldsymbol{K}}^{-1}\tilde{\boldsymbol{\sigma}}_h^{i,\mathrm{m}}\right) \\ & + \left((\underline{\boldsymbol{K}}\nabla s_h^i + \boldsymbol{\sigma}_h^i)\cdot\boldsymbol{n}, \tilde{u}_{\mathrm{D}}\right)_{\Gamma_{\mathrm{D}}} + Q(s_h^i - u_h^i). \end{aligned} \tag{4.17}$$

By Definition (4.15) of the average flux $\tilde{\boldsymbol{\sigma}}_h^{i,\mathrm{m}}$, we observe that

$$\begin{aligned} & \|\underline{\boldsymbol{K}}\nabla\tilde{u} + \tilde{\boldsymbol{\sigma}}_h^{i,\mathrm{m}}\|^2_{\underline{\boldsymbol{K}}^{-\frac{1}{2}}} = \frac{1}{4}\|\underline{\boldsymbol{K}}\nabla(\tilde{u} - \tilde{s}_h^i) + \left(\underline{\boldsymbol{K}}\nabla\tilde{u} + \tilde{\boldsymbol{\sigma}}_h^i\right)\|^2_{\underline{\boldsymbol{K}}^{-\frac{1}{2}}} \\ = & \frac{1}{4}\|\underline{\boldsymbol{K}}\nabla(\tilde{u} - \tilde{s}_h^i)\|^2_{\underline{\boldsymbol{K}}^{-\frac{1}{2}}} + \frac{1}{4}\|\underline{\boldsymbol{K}}\nabla\tilde{u} + \tilde{\boldsymbol{\sigma}}_h^i\|^2_{\underline{\boldsymbol{K}}^{-\frac{1}{2}}} + \frac{1}{2}(\underline{\boldsymbol{K}}^{\frac{1}{2}}\nabla(\tilde{u} - \tilde{s}_h^i), \underline{\boldsymbol{K}}^{\frac{1}{2}}\nabla\tilde{u} + \underline{\boldsymbol{K}}^{-\frac{1}{2}}\tilde{\boldsymbol{\sigma}}_h^i). \end{aligned} \tag{4.18}$$

The symmetry of $\underline{\boldsymbol{K}}$, the Green formula, (3.5) which implies that $-\underline{\boldsymbol{K}}\nabla\tilde{u} \in \boldsymbol{H}(\mathrm{div}\,,\Omega)$ with divergence $-\nabla\cdot(\underline{\boldsymbol{K}}\nabla\tilde{u}) = \tilde{f}$, (4.2b), (4.1c), and (4.2c) lead to

$$\begin{aligned} & (\underline{\boldsymbol{K}}^{\frac{1}{2}}\nabla(\tilde{u} - \tilde{s}_h^i), \underline{\boldsymbol{K}}^{\frac{1}{2}}\nabla\tilde{u} + \underline{\boldsymbol{K}}^{-\frac{1}{2}}\tilde{\boldsymbol{\sigma}}_h^i) = (\nabla(\tilde{u} - \tilde{s}_h^i), \underline{\boldsymbol{K}}\nabla\tilde{u} + \tilde{\boldsymbol{\sigma}}_h^i) \\ = & -\left(\tilde{u} - \tilde{s}_h^i, \nabla\cdot(\underline{\boldsymbol{K}}\nabla\tilde{u} + \tilde{\boldsymbol{\sigma}}_h^i)\right) + (\tilde{u} - \tilde{s}_h^i, (\underline{\boldsymbol{K}}\nabla\tilde{u} + \tilde{\boldsymbol{\sigma}}_h^i)\cdot\boldsymbol{n})_{\partial\Omega} = 0. \end{aligned}$$

This and the Prager–Synge equality (4.4) that we employ in (4.18) lead to

$$\|\underline{\boldsymbol{K}}\nabla\tilde{u} + \tilde{\boldsymbol{\sigma}}_h^{i,\mathrm{m}}\|^2_{\underline{\boldsymbol{K}}^{-\frac{1}{2}}} = \frac{1}{4}\|\underline{\boldsymbol{K}}\nabla\tilde{s}_h^i + \tilde{\boldsymbol{\sigma}}_h^i\|^2_{\underline{\boldsymbol{K}}^{-\frac{1}{2}}}. \tag{4.19}$$

Moving the second term of the right-hand side of (4.17) to the left-hand side and applying the Cauchy–Schwarz inequality together with (4.19) concludes the proof. □

Remark 4.9 (Modified goal error)**.** *It is claimed and numerically illustrated in [28–30], see also the references therein, that the modified goal error* $\left|Q(u) - Q(u_h^i) - \left(\underline{\boldsymbol{K}}\nabla s_h^i + \boldsymbol{\sigma}_h^i, \underline{\boldsymbol{K}}^{-1}\tilde{\boldsymbol{\sigma}}_h^{i,\mathrm{m}}\right)\right|$ *is often smaller than the original goal error* $|Q(u) - Q(u_h^i)|$*. This is, however, not always the case, as we illustrate it numerically in Section 6.4 below. The illustration in Section 6.4, though, indeed shows that modified estimate of the modified error* (4.16) *is much sharper than the simple estimate of the error* (4.14) *(in terms of effectivity indices). Please also note that, unfortunately, both goal estimators* (4.14) *and* (4.16) *can be nonzero while bounding a zero goal error, see Section 6.5 below.*

Remark 4.10 (Galerkin orthogonality)**.** *The derivation of estimate* (4.16) *does not involve any Galerkin orthogonality. This is replaced here by the necessity to obtain an equilibrated flux reconstruction in the sense of Definition 4.2, see in particular* (4.2b).

One specific advantage of our approach is that one can consider same or different (order of) finite element approximations of the primal and dual problems. This stands in contrast to usual residual-type estimators, cf., e.g., [33] and the references therein that use the Galerkin orthogonality (often one of the primal and dual discrete spaces should be strictly contained in the other discrete space).

4.4 Discretization and algebraic error flux reconstructions

We will below consider numerical discretizations of (3.2) and (3.5) with inexact solutions of the arising linear systems. In such a context, it is not obvious at all to obtain (4.2b). We now outline a framework allowing to do so, following Papež *et al.* [37] and the references therein.

The idea is to split the flux reconstruction $\boldsymbol{\sigma}_h^i$ of Definition 4.2 to a discretization flux reconstruction $\boldsymbol{\sigma}_{h,\mathrm{disc}}^i$ and an algebraic error flux reconstruction $\boldsymbol{\sigma}_{h,\mathrm{alg}}^i$. The latter reconstruction has to disappear for an exact solver, and is solely defined from the algebraic residual of the discrete primal problem represented by a discontinuous piecewise polynomial $r_h^i \in \mathbb{P}_p(\mathcal{T}_h)$ or $r_h^i \in \mathbb{Q}_p(\mathcal{T}_h)$. A similar decomposition is performed for the dual problem:

Assumption 4.11 (Discretization flux reconstruction)**.** *There exist a piecewise polynomial vector-valued function $\boldsymbol{\sigma}_{h,\mathrm{disc}}^i$ (resp. $\tilde{\boldsymbol{\sigma}}_{h,\mathrm{disc}}^i$) locally constructed from u_h^i and r_h^i (resp. $\tilde{u}_h^i$ and $\tilde{r}_h^i$) which satisfies*

$$\boldsymbol{\sigma}_{h,\mathrm{disc}}^i \in \boldsymbol{RTN}_p(\Omega) \quad (\textit{resp. } \tilde{\boldsymbol{\sigma}}_{h,\mathrm{disc}}^i \in \boldsymbol{RTN}_p(\Omega)), \tag{4.20a}$$

$$\nabla\cdot\boldsymbol{\sigma}_{h,\mathrm{disc}}^i = f - r_h^i \quad (\textit{resp. } \nabla\cdot\tilde{\boldsymbol{\sigma}}_{h,\mathrm{disc}}^i = \tilde{f} - \tilde{r}_h^i) \quad \textit{in } \Omega, \tag{4.20b}$$

$$\boldsymbol{\sigma}_{h,\mathrm{disc}}^i\cdot\boldsymbol{n} = \sigma_{\mathrm{N}} \quad (\textit{resp. } \tilde{\boldsymbol{\sigma}}_{h,\mathrm{disc}}^i\cdot\boldsymbol{n} = 0) \quad \textit{on } \Gamma_{\mathrm{N}} \qquad \textit{when } \Gamma_{\mathrm{N}} \neq \emptyset. \tag{4.20c}$$

Assumption 4.12 (Algebraic error flux reconstruction (lifting of the algebraic residual))**.** *There exists an algebraic error flux reconstruction $\boldsymbol{\sigma}_{h,\mathrm{alg}}^i$ (resp. $\tilde{\boldsymbol{\sigma}}_{h,\mathrm{alg}}^i$) cheaply constructed from r_h^i (resp. $\tilde{r}_h^i$) which satisfies*

$$\boldsymbol{\sigma}_{h,\mathrm{alg}}^i \in \boldsymbol{RTN}_p(\Omega) \quad (\textit{resp. } \tilde{\boldsymbol{\sigma}}_{h,\mathrm{alg}}^i \in \boldsymbol{RTN}_p(\Omega)), \tag{4.21a}$$

$$\nabla\cdot\boldsymbol{\sigma}_{h,\mathrm{alg}}^i = r_h^i \quad (\textit{resp. } \nabla\cdot\tilde{\boldsymbol{\sigma}}_{h,\mathrm{alg}}^i = \tilde{r}_h^i) \quad \textit{in } \Omega, \tag{4.21b}$$

$$\boldsymbol{\sigma}_{h,\mathrm{alg}}^i\cdot\boldsymbol{n} = 0 \quad (\textit{resp. } \tilde{\boldsymbol{\sigma}}_{h,\mathrm{alg}}^i\cdot\boldsymbol{n} = 0) \quad \textit{on } \Gamma_{\mathrm{N}} \qquad \textit{when } \Gamma_{\mathrm{N}} \neq \emptyset. \tag{4.21c}$$

Assumption 4.11 is verified in all the applications below. Assumption 4.12 can on its turn be verified independently of the numerical discretization and the algebraic solver at hand following Papež *et al.* [37]. We provide a brief outline of this procedure in Appendix 8. With these decompositions, the goal-oriented a posteriori error estimate of Theorem 4.8 can further distinguish the error components in terms of numerical discretization and linear algebra:

Theorem 4.13 (A posteriori error estimate distinguishing the discretization and algebraic error components)**.** *Let the hypotheses of Theorem 4.8 be satisfied and let Assumptions 4.11 and 4.12 hold. Then*

$$\begin{aligned}
&\left|Q(u) - Q(u_h^i) - \left(\underline{\boldsymbol{K}}\nabla s_h^i + \boldsymbol{\sigma}_h^i, \underline{\boldsymbol{K}}^{-1}\tilde{\boldsymbol{\sigma}}_h^{i,\mathrm{m}}\right)\right| \\
&\le \frac{1}{2}\left(\|\underline{\boldsymbol{K}}\nabla s_h^i + \boldsymbol{\sigma}_{h,\mathrm{disc}}^i\|_{\underline{\boldsymbol{K}}^{-\frac{1}{2}}} + \|\boldsymbol{\sigma}_{h,\mathrm{alg}}^i\|_{\underline{\boldsymbol{K}}^{-\frac{1}{2}}}\right)\left(\|\underline{\boldsymbol{K}}\nabla \tilde{s}_h^i + \tilde{\boldsymbol{\sigma}}_{h,\mathrm{disc}}^i\|_{\underline{\boldsymbol{K}}^{-\frac{1}{2}}} + \|\tilde{\boldsymbol{\sigma}}_{h,\mathrm{alg}}^i\|_{\underline{\boldsymbol{K}}^{-\frac{1}{2}}}\right) \\
&\quad + \left|\left((\underline{\boldsymbol{K}}\nabla s_h^i + \boldsymbol{\sigma}_{h,\mathrm{disc}}^i)\cdot\boldsymbol{n}, \tilde{u}_{\mathrm{D}}\right)_{\Gamma_{\mathrm{D}}}\right| + \left|\left(\boldsymbol{\sigma}_{h,\mathrm{alg}}^i\cdot\boldsymbol{n}, \tilde{u}_{\mathrm{D}}\right)_{\Gamma_{\mathrm{D}}}\right| + \left|Q(s_h^i - u_h^i)\right|.
\end{aligned} \tag{4.22}$$

5 Applications to discretization methods

We show now the applications of the a posteriori estimate established in Section 4 to various finite element and finite volume methods.

Here and throughout the next sections, the construction of the discrete potential $\tilde{s}_h^i \in H^1_{\tilde{u}_{\mathrm{D}}}(\Omega)$ of Definition 4.1 and of the reconstructed flux $\tilde{\boldsymbol{\sigma}}_h^i \in \boldsymbol{RTN}_p(\Omega)$ of Definition 4.2 related to the dual problem are obtained exactly in the same way as the constructions of $s_h^i \in H^1_{u_{\mathrm{D}}}(\Omega)$ and $\boldsymbol{\sigma}_h^i \in \boldsymbol{RTN}_p(\Omega)$ related to the primal problem by setting $\sigma_{\mathrm{N}} = 0$ on Γ_{N}, and replacing u_{D} by $\tilde{u}_{\mathrm{D}}$ and f by $\tilde{f}$. Similarly, we henceforth only present details on simplicial meshes $\mathcal{T}_h$.

5.1 Conforming finite elements

In this section, we describe the conforming finite element method and the the corresponding flux reconstructions. Let $V_h := \mathbb{P}_p(\mathcal{T}_h) \cap H^1_{\mathrm{D}}(\Omega)$. The discrete formulation of (3.2) seeks $u_{h,0} \in V_h$ such that

$$(\underline{\boldsymbol{K}} \nabla u_{h,0}, \nabla v_h) = (f, v_h) - (\sigma_{\mathrm{N}}, v_h)_{\Gamma_{\mathrm{N}}} - (\underline{\boldsymbol{K}} \nabla u_{\mathrm{D}}, \nabla v_h) \quad \forall v_h \in V_h \tag{5.1}$$

and one sets $u_h := u_{h,0} + u_{\mathrm{D}}$.

Let $\psi_h^l, 1 \le l \le N_h$, form a basis of V_h. Then the discrete problem (5.1) is equivalent to solving a system of linear algebraic equations with a symmetric positive definite matrix: find $\mathsf{U}_h \in \mathbb{R}^{N_h}$ such that

$$\mathbb{A}\mathsf{U}_h = \mathsf{F}_h, \tag{5.2}$$

where

$$\begin{aligned}(\mathbb{A})_{lm} &:= (\underline{\boldsymbol{K}} \nabla \psi_h^m, \nabla \psi_h^l),\\ (\mathsf{F}_h)_l &:= (f, \psi_h^l) - (\sigma_{\mathrm{N}}, \psi_h^l)_{\Gamma_{\mathrm{N}}} - (\underline{\boldsymbol{K}} \nabla u_{\mathrm{D}}, \nabla \psi_h^l).\end{aligned}$$

Then $u_{h,0} := \sum_{m=1}^{N_h} (\mathsf{U}_h)_m \psi_h^m \in V_h$. Let $\mathsf{U}_h^i \in \mathbb{R}^{N_h}$ be an arbitrary approximation of the exact solution U_h of (5.2) which corresponds to an arbitrary approximation $u_{h,0}^i$ of (5.1) with $u_{h,0}^i = \sum_{m=1}^{N_h} (\mathsf{U}_h^i)_m \psi_h^m \in V_h$; then $u_h^i := u_{h,0}^i + u_{\mathrm{D}}$. The algebraic residual vector is

$$\mathsf{R}_h^i := \mathsf{F}_h - \mathbb{A}\mathsf{U}_h^i. \tag{5.3}$$

Following [37, 38], we associate R_h^i with an elementwise discontinuous polynomial r_h^i of degree p, vanishing on the Dirichlet boundary Γ_{D}. Let N_h^l be the number of elements forming the support of the basis function $\psi_h^l, 1 \le l \le N_h$. For each fixed element $K \in \mathcal{T}_h$, we define $r_h^i|_K \in \mathbb{P}_p(K)$ by

$$(r_h^i, \psi_h^l)_K = \frac{(\mathsf{R}_h^i)_l}{N_h^l}, \quad r_h^i|_{\partial K \cap \Gamma_{\mathrm{D}}} = 0, \tag{5.4}$$

for all basis functions ψ_h^l of the space V_h non-vanishing on K. Such r_h^i satisfies $(\mathsf{R}_h^i)_l = (r_h^i, \psi_h^l), 1 \le l \le N_h$, and the algebraic relation (5.3) yields

$$(r_h^i, v_h) = (f, v_h) - (\sigma_{\mathrm{N}}, v_h)_{\Gamma_{\mathrm{N}}} - (\underline{\boldsymbol{K}} \nabla u_h^i, \nabla v_h) \quad \forall v_h \in V_h. \tag{5.5}$$

In view of the fact that u_h^i is conforming since $V_h \subset H^1_{\mathrm{D}}(\Omega)$, we can directly set $s_h^i := u_h^i$ to obtain a potential reconstruction in the sense of Definition 4.1. As for the flux reconstruction in the sense of Definition 4.2, let $\psi_h^{\boldsymbol{a}} \in \mathbb{P}_1(\mathcal{T}_h) \cap H^1(\Omega)$ stand for the hat basis function associated with a vertex $\boldsymbol{a} \in \mathcal{V}_h$. For all vertices $\boldsymbol{a} \in \mathcal{V}_h$, let $\mathcal{T}_h^{\boldsymbol{a}}$ be the patch of elements of $\mathcal{T}_h$ that share $\boldsymbol{a}$. Moreover, $\omega_h^{\boldsymbol{a}}$ is the corresponding open subdomain, forming the support of hat basis function $\psi_h^{\boldsymbol{a}}$. Let $\boldsymbol{RTN}_p^{\mathrm{N},0}(\omega_h^{\boldsymbol{a}})$ be the subspace of $\boldsymbol{RTN}_p(\Omega)$ restricted to $\omega_h^{\boldsymbol{a}}$ with zero normal flux through $\partial\omega_h^{\boldsymbol{a}}$ for an interior vertex $\boldsymbol{a} \in \mathcal{V}_h^{\mathrm{int}}$ or a vertex in the interior of the Neumann boundary $\boldsymbol{a} \in \mathcal{V}_h^{\mathrm{N}}$ and zero normal flux through that part of $\partial\omega_h^{\boldsymbol{a}}$ which lies inside Ω and on Γ_{N} for $\mathcal{V}_h^{\mathrm{D}}$. For interior vertices, let $\boldsymbol{RTN}_p^{\mathrm{N},\sigma_{\mathrm{N}}}(\omega_h^{\boldsymbol{a}}) := \boldsymbol{RTN}_p^{\mathrm{N},0}(\omega_h^{\boldsymbol{a}})$, whereas for boundary vertices, we also need the space $\boldsymbol{RTN}_p^{\mathrm{N},\sigma_{\mathrm{N}}}(\omega_h^{\boldsymbol{a}})$ where the normal component over Γ_{N} is imposed by the projection of $\sigma_{\mathrm{N}}\psi_h^{\boldsymbol{a}}$ to piecewise p-degree polynomials. Let $\mathbb{P}_p^*(\mathcal{T}_h^{\boldsymbol{a}})$ be the subspace of discontinuous piecewise polynomials $\mathbb{P}_p(\mathcal{T}_h^{\boldsymbol{a}})$ with zero mean on $\omega_h^{\boldsymbol{a}}$ when $\boldsymbol{a} \in \mathcal{V}_h^{\mathrm{int}}$ or $\boldsymbol{a} \in \mathcal{V}_h^{\mathrm{N}}$, and $\mathbb{P}_p(\mathcal{T}_h^{\boldsymbol{a}})$ otherwise. Then, the discretization flux reconstruction $\boldsymbol{\sigma}_{h,\mathrm{disc}}^i$ is computed by the following local patchwise problems, see [6, 10, 12, 37] for more details:

Definition 5.1 (Discretization flux reconstruction $\boldsymbol{\sigma}_{h,\mathrm{disc}}^i$)**.** *For all vertices $\boldsymbol{a} \in \mathcal{V}_h$, define $\boldsymbol{\sigma}_{h,\mathrm{dis}}^{i,\boldsymbol{a}} \in \boldsymbol{RTN}_p^{\mathrm{N},\sigma_\mathrm{N}}(\omega_h^{\boldsymbol{a}})$ and $\gamma_h^{\boldsymbol{a}} \in \mathbb{P}_p^*(\mathcal{T}_h^{\boldsymbol{a}})$ by*

$$(\boldsymbol{\sigma}_{h,\mathrm{dis}}^{i,\boldsymbol{a}}, \boldsymbol{v}_h)_{\omega_h^{\boldsymbol{a}}} - (\gamma_h^{\boldsymbol{a}}, \nabla\cdot\boldsymbol{v}_h)_{\omega_h^{\boldsymbol{a}}} = -(\psi_h^{\boldsymbol{a}}\underline{\boldsymbol{K}}\nabla u_h^i, \boldsymbol{v}_h)_{\omega_h^{\boldsymbol{a}}} \qquad \forall \boldsymbol{v}_h \in \boldsymbol{RTN}_p^{\mathrm{N},0}(\omega_h^{\boldsymbol{a}}), \tag{5.6a}$$

$$(\nabla\cdot\boldsymbol{\sigma}_{h,\mathrm{dis}}^{i,\boldsymbol{a}}, q_h)_{\omega_h^{\boldsymbol{a}}} = (f\psi_h^{\boldsymbol{a}} - r_h^i\psi_h^{\boldsymbol{a}} - \underline{\boldsymbol{K}}\nabla u_h^i\cdot\nabla\psi_h^{\boldsymbol{a}}, q_h)_{\omega_h^{\boldsymbol{a}}} \qquad \forall q_h \in \mathbb{P}_p^*(\mathcal{T}_h^{\boldsymbol{a}}). \tag{5.6b}$$

Then set

$$\boldsymbol{\sigma}_{h,\mathrm{dis}}^i := \sum_{\boldsymbol{a}\in\mathcal{V}_h} \boldsymbol{\sigma}_{h,\mathrm{dis}}^{i,\boldsymbol{a}} \in \boldsymbol{RTN}_p(\Omega). \tag{5.6c}$$

The Neumann compatibility condition for (5.6) amounts to

$$(f - r_h^i, \psi_h^{\boldsymbol{a}}) - (\sigma_\mathrm{N}, \psi_h^{\boldsymbol{a}})_{\Gamma_\mathrm{N}} - (\underline{\boldsymbol{K}}\nabla u_h^i, \nabla\psi_h^{\boldsymbol{a}}) = 0 \quad \forall \boldsymbol{a} \in \mathcal{V}_h^{\mathrm{int}} \cup \mathcal{V}_h^{\mathrm{N}} \tag{5.7}$$

and follows from (5.5).

In view of the definition of the residual r_h^i in (5.4) and its key property (5.5) together with Definition 5.1, there holds, cf. [6, 10, 12, 37]:

Lemma 5.2 (Assumption 4.11)**.** *Let the pair (u_h^i, r_h^i) be given by (5.1)–(5.4) and $\boldsymbol{\sigma}_{h,\mathrm{disc}}^i$ by Definition 5.1. Then Assumption 4.11 holds.*

5.2 Nonconforming finite elements

Let V_h stand for the space of functions v_h from $\mathbb{P}_p(\mathcal{T}_h), p \geq 1$, satisfying the jump orthogonality

$$(\llbracket v_h \rrbracket_e, q_h)_e = 0 \quad \forall q_h \in \mathbb{P}_{p-1}(e), \quad \forall e \in \mathcal{E}_h^{\mathrm{int}} \cup \mathcal{E}_h^{\mathrm{D}}. \tag{5.8}$$

The nonconforming finite element discretization of (3.2) looks for $u_{h,0} \in V_h$ such that

$$(\underline{\boldsymbol{K}}\nabla u_{h,0}, \nabla v_h) = (f, v_h) - (\sigma_\mathrm{N}, v_h)_{\Gamma_\mathrm{N}} - (\underline{\boldsymbol{K}}\nabla \bar{u}_\mathrm{D}, \nabla v_h) \quad \forall v_h \in V_h, \tag{5.9}$$

where $\bar{u}_\mathrm{D}$ is the nonconforming finite element approximation of the Dirichlet datum u_D; one sets $u_h := u_{h,0} + \bar{u}_\mathrm{D}$. Energy a posteriori error estimates are derived in particular in [1, 20], see also the references therein. Algebraically, (5.9) is rewritten as: find $\mathsf{U}_h \in \mathbb{R}^{N_h}$ such that $\mathbb{A}\mathsf{U}_h = \mathsf{F}_h$, and the algebraic residual vector $\mathsf{R}_h^i := \mathsf{F}_h - \mathbb{A}\mathsf{U}_h^i$ is used to construct an elementwise discontinuous polygonal r_h^i of degree p vanishing on Γ_D as above, such that (5.5) holds.

Since the lowest-order conforming hat functions $\psi_h^{\boldsymbol{a}}$ belong to the nonconforming space V_h for all vertices $\boldsymbol{a} \in \mathcal{V}_h^{\mathrm{int}} \cup \mathcal{V}_h^{\mathrm{N}}$, so that (5.7) holds, the discretization flux reconstruction $\boldsymbol{\sigma}_{h,\mathrm{disc}}^i$ can be prescribed by Definition 5.1. Hence, it follows immediately that:

Lemma 5.3 (Assumption 4.11)**.** *Let the pair (u_h^i, r_h^i) be as described above and let $\boldsymbol{\sigma}_{h,\mathrm{disc}}^i$ be given by Definition 5.1. Then Assumption 4.11 is satisfied.*

Remark 5.4 (Alternative flux reconstruction in the lowest-order case)**.** *Let $f \in \mathbb{P}_0(\mathcal{T}_h)$ and $\sigma_\mathrm{N} \in \mathbb{P}_0(\mathcal{E}_h^\mathrm{N})$ be piecewise constant for simplicity. Then, for the case $p = 1$, one can simply prescribe the flux reconstruction $\boldsymbol{\sigma}_{h,\mathrm{disc}}$ element by element as follows. For $K \in \mathcal{T}_h$, define $\boldsymbol{f}_h(\boldsymbol{x})|_K := \frac{f|_K}{d}(\boldsymbol{x} - \boldsymbol{x}_K)$ with $\boldsymbol{x}_K$ the barycenter of K. For each face $e \in \mathcal{E}_K$, let $\boldsymbol{a}_{K,e}$ be the vertex of K opposite to e. Let $\mathcal{T}_h^e$ stand for the patch of (one or two) elements sharing the face e. Following [18, 19], set*

$$\boldsymbol{\sigma}_{h,\mathrm{disc}}^i|_K := -\underline{\boldsymbol{K}}\nabla u_h^i|_K + \boldsymbol{f}_h(\boldsymbol{x})|_K - \sum_{e\in\mathcal{E}_K} |\mathcal{T}_h^e|^{-1}\frac{\mathsf{R}_e^i}{d}(\boldsymbol{x} - \boldsymbol{a}_{K,e}), \tag{5.10}$$

where $\mathsf{R}_e^i := (f,\psi_e) - (\sigma_{\rm N},\psi_e)_{\Gamma_{\rm N}} - (\underline{\boldsymbol{K}}\nabla u_h^i,\nabla\psi_e)$ *for all* $e\in\mathcal{E}_h^{\rm int}\cup\mathcal{E}_h^{\rm N}$*, with* ψ_e *being the face basis functions of* V_h *for* $p=1$*. The algebraic residual function is then elementwise constant and defined by* $r_h^i|_K := \sum_{e\in\mathcal{E}_K}|\mathcal{T}_h^e|^{-1}\mathsf{R}_e^i$*. It can be verified that this construction also satisfies Assumption 4.11 (actually* $\boldsymbol{\sigma}_{h,\rm disc}^i\in\boldsymbol{RTN}_0(\Omega)$*), see [18, Lemma 6.5].*

There are numerous possibilities to obtain a potential reconstruction in the sense of Definition 4.1. The following is a slightly cheaper variant of [20, Construction 3.8 and Remark 3.10], where $(p+1)$-degree piecewise polynomials are used in place of the present $s_h^i\in H^1(\Omega)\cap\mathbb{P}_p(\mathcal{T}_h)$:

Definition 5.5 (Potential reconstruction by local minimizations)**.** *For an interior vertex* $\boldsymbol{a}\in\mathcal{V}_h^{\rm int}$*, let* $V^{{\rm D},0}(\omega_h^{\boldsymbol{a}}) := \mathbb{P}_p(\mathcal{T}_h^{\boldsymbol{a}})\cap H_0^1(\omega_h^{\boldsymbol{a}})$*. For a boundary vertex* $\boldsymbol{a}\in\mathcal{V}_h^{\rm ext}$*, let* $V^{{\rm D},0}(\omega_h^{\boldsymbol{a}})$ *be the subspace of* $\mathbb{P}_p(\mathcal{T}_h^{\boldsymbol{a}})\cap H^1(\omega_h^{\boldsymbol{a}})$ *with zero trace on that part of* $\partial\omega_h^{\boldsymbol{a}}$ *which lies inside* Ω *and on* $\Gamma_{\rm D}$*. For interior vertices, let* $V^{{\rm D},u_{\rm D}}(\omega_h^{\boldsymbol{a}}) := V^{{\rm D},0}(\omega_h^{\boldsymbol{a}})$*, whereas for boundary vertices, we also need the space* $V^{{\rm D},u_{\rm D}}(\omega_h^{\boldsymbol{a}})$ *where the trace on* $\Gamma_{\rm D}$ *is imposed by the projection of* $u_{\rm D}\psi_h^{\boldsymbol{a}}$ *to piecewise* p*-degree polynomials. We define* $s_h^{i,\boldsymbol{a}}\in V^{{\rm D},u_{\rm D}}(\omega_h^{\boldsymbol{a}})$ *such that*

$$(\underline{\boldsymbol{K}}\nabla s_h^{i,\boldsymbol{a}},\nabla v_h)_{\omega_h^{\boldsymbol{a}}} = (\underline{\boldsymbol{K}}\nabla(\psi_{\boldsymbol{a}}u_h),\nabla v_h)_{\omega_h^{\boldsymbol{a}}}\qquad\forall v_h\in V^{{\rm D},0}(\omega_h^{\boldsymbol{a}}),\tag{5.11a}$$

and the potential reconstruction is obtained by

$$s_h^i := \sum_{\boldsymbol{a}\in\mathcal{V}_h} s_h^{i,\boldsymbol{a}}.\tag{5.11b}$$

It is also possible to prescribe directly the degrees of freedom, without any solution of local problems, following [26] and the references therein:

Definition 5.6 (Potential reconstruction by local averaging)**.** *Let the averaging operator* $\mathcal{I}_{\rm av}:\mathbb{P}_p(\mathcal{T}_h)\to\mathbb{P}_p(\mathcal{T}_h)\cap H^1_{u_{\rm D}}(\Omega)$ *be such that, for any* $v_h\in\mathbb{P}_p(\mathcal{T}_h)$*, the values of* $\mathcal{I}_{\rm av}(v_h)$ *are prescribed at the Lagrange interpolation nodes* $\boldsymbol{x}$ *of the conforming finite element space* $\mathbb{P}_p(\mathcal{T}_h)\cap H^1_{u_{\rm D}}(\Omega)$ *by*

$$\mathcal{I}_{\rm av}(v_h)(\boldsymbol{x}) := \begin{cases}\dfrac{1}{{\rm card}(\mathcal{T}_h^{\boldsymbol{x}})}\displaystyle\sum_{K\in\mathcal{T}_h^{\boldsymbol{x}}}(v_h|_K)(\boldsymbol{x}) & \boldsymbol{x}\in\Omega,\\ u_{\rm D}(\boldsymbol{x}) & \boldsymbol{x}\in\overline{\Gamma}_{\rm D},\end{cases}\tag{5.12}$$

where $\mathcal{T}_h^{\boldsymbol{x}}$ *regroups all the mesh elements* $K\in\mathcal{T}_h$ *sharing* $\boldsymbol{x}$*. The potential reconstruction is given by*

$$s_h^i := \mathcal{I}_{\rm av}(u_h^i).\tag{5.13}$$

5.3 Discontinuous Galerkin elements

In this section, we consider the discontinuous Galerkin method for problem (3.2). For non-negative weights $w_{K^\mp,e}$ that can be chosen as $w_{K^\mp,e} = (\delta_{\underline{\boldsymbol{K}},e^+}+\delta_{\underline{\boldsymbol{K}},e^-})^{-1}\delta_{\underline{\boldsymbol{K}},e^\pm}$ with $\delta_{\underline{\boldsymbol{K}},e^\pm} = \boldsymbol{n}_e^t\underline{\boldsymbol{K}}|_{K^\pm}\boldsymbol{n}_e$, define the weighted average of v on interior face $e\in\mathcal{E}_h^{\rm int}$ by $\{\!\{v\}\!\}_{\rm w} := \big(w_{K^+,e}v|_{K^+}+w_{K^-,e}v|_{K^-}\big)$ and on boundary face $e\in\mathcal{E}_h^{\rm ext}$ with $e=\partial K\cap\Gamma$ by $\{\!\{v\}\!\}_{\rm w} := v|_K$. Then the discontinuous Galerkin method seeks $u_h\in V_h := \mathbb{P}_p(\mathcal{T}_h)$ with $p\ge1$ such that

$$\begin{aligned}&(\underline{\boldsymbol{K}}\nabla u_h,\nabla v_h) - \sum_{e\in\mathcal{E}_h^{\rm int}\cup\mathcal{E}_h^{\rm D}}\Big\{(\{\!\{\underline{\boldsymbol{K}}\nabla u_h\cdot\boldsymbol{n}\}\!\}_{\rm w},[\![v_h]\!])_e + \vartheta(\{\!\{\underline{\boldsymbol{K}}\nabla v_h\cdot\boldsymbol{n}\}\!\}_{\rm w},[\![u_h]\!])_e - \xi\frac{\gamma_{\underline{\boldsymbol{K}},e}}{h_e}([\![u_h]\!],[\![v_h]\!])_e\Big\}\\ &= (f,v_h) - (\sigma_{\rm N},v_h)_{\Gamma_{\rm N}} - \sum_{e\in\mathcal{E}_h^{\rm D}}\Big\{\vartheta\,(u_{\rm D},\underline{\boldsymbol{K}}\nabla v_h\cdot\boldsymbol{n})_e - \xi\frac{\gamma_{\underline{\boldsymbol{K}},e}}{h_e}(u_{\rm D},v_h)_e\Big\}\quad\forall v_h\in V_h,\end{aligned}\tag{5.14}$$

where ξ is a sufficiently large positive penalty parameter, $\vartheta \in \{-1, 0, 1\}$, and the penalty coefficient $\gamma_{\underline{\boldsymbol{K}},e}$ is defined on interior faces e as $\gamma_{\underline{\boldsymbol{K}},e} := (\delta_{\underline{\boldsymbol{K}},e^+} + \delta_{\underline{\boldsymbol{K}},e^-})^{-1}\delta_{\underline{\boldsymbol{K}},e^+}\delta_{\underline{\boldsymbol{K}},e^-}$ and as $\gamma_{\underline{\boldsymbol{K}},e} := \delta_{\underline{\boldsymbol{K}},e}$ on boundary faces. Denote the basis functions of V_h by $\psi_{K,j}$ for all $K \in \mathcal{T}_h$ and all $j \in \{1, \ldots, N\}, N := \dim(\mathbb{P}_p(K))$. Then the matrix formulation of (5.14) is: find $\mathsf{U}_h \in \mathbb{R}^{\mathrm{card}(\mathcal{T}_h)\times N}$ such that

$$\mathbb{A}\mathsf{U}_h = \mathsf{F}_h \tag{5.15}$$

and the algebraic residual equation on iteration i writes

$$\mathsf{R}_h^i := \mathsf{F}_h - \mathbb{A}\mathsf{U}_h^i. \tag{5.16}$$

We finally define the algebraic residual function $r_h^i \in \mathbb{P}_p(\mathcal{T}_h)$ by, for element $K \in \mathcal{T}_h$ and $j \in \{1, \ldots, N\}$,

$$(r_h^i, \psi_{K,j})_K = (\mathsf{R}_h^i)_{K,j}. \tag{5.17}$$

We can obtain a discretization flux reconstruction $\boldsymbol{\sigma}_{h,\mathrm{dis}}^i \in \boldsymbol{RTN}_p(\Omega)$ by Definition 5.1 when the parameter $\vartheta = 0$, which ensures the Neumann compatibility condition (5.7); indeed, it is enough to consider $v_h = \psi_h^{\boldsymbol{a}}$ in (5.14) in this case. For $\vartheta = -1, 1$, such a construction is also possible after a slight modification of the broken gradient ∇u_h^i into the so-called discrete gradient, cf. [11, 20]. One can also directly prescribe the degrees of freedom of the discretization flux reconstruction $\boldsymbol{\sigma}_{h,\mathrm{disc}}^i$ following [14, 17, 18] as follows:

Definition 5.7 (Flux reconstruction by direct prescription)**.** *Let in this definition* $[\![u_h^i]\!] := u_h^i - u_{\mathrm{D}}$ *on Dirichlet boundary faces* $e \in \mathcal{E}_h^{\mathrm{D}}$*. For given* $u_h^i \in \mathbb{P}_p(\mathcal{T}_h)$*, define the discretization flux reconstruction* $\boldsymbol{\sigma}_{h,\mathrm{dis}}^i \in \boldsymbol{RTN}_p(\Omega)$ *such that, for all* $K \in \mathcal{T}_h$*,*

$$(\boldsymbol{\sigma}_{h,\mathrm{dis}}^i \cdot \boldsymbol{n}_e, v_e)_e := (-\{\!\{\underline{\boldsymbol{K}}\nabla u_h^i \cdot \boldsymbol{n}_e\}\!\}_{\mathrm{w}} + \xi \frac{\gamma_{\underline{\boldsymbol{K}},e}}{h_e}[\![u_h^i]\!], v_e)_e \qquad \forall v_e \in \mathbb{P}_p(e),\ \forall e \in \mathcal{E}_K \cap (\mathcal{E}_h^{\mathrm{int}} \cup \mathcal{E}_h^{\mathrm{D}}), \tag{5.18}$$

$$(\boldsymbol{\sigma}_{h,\mathrm{dis}}^i \cdot \boldsymbol{n}_e, v_e)_e := (\sigma_{\mathrm{N}}, v_e)_e \qquad \forall v_e \in \mathbb{P}_p(e),\ \forall e \in \mathcal{E}_K \cap \mathcal{E}_h^{\mathrm{N}}, \tag{5.19}$$

$$(\boldsymbol{\sigma}_{h,\mathrm{dis}}^i, \boldsymbol{t}_h)_K := -(\underline{\boldsymbol{K}}\nabla u_h^i, \boldsymbol{t}_h)_K + \vartheta \sum_{e \in \mathcal{E}_K \setminus \mathcal{E}_h^{\mathrm{N}}} (\chi_{K,e}[\![u_h^i]\!], \underline{\boldsymbol{K}}\boldsymbol{t}_h \cdot \boldsymbol{n}_e)_e \ \forall \boldsymbol{t}_h \in [\mathbb{P}_{p-1}(K)]^d, \tag{5.20}$$

where $\chi_{K,e} = w_{K,e}$ *if* $e \in \mathcal{E}_h^{\mathrm{int}}$ *and* $\chi_{K,e} = 1$ *if* $e \in \mathcal{E}_h^{\mathrm{ext}}$*.*

Assumption 4.11 now follows from the definition of discretization flux reconstruction and the definition of residual function r_h^i:

Lemma 5.8 (Assumption 4.11)**.** *Let the pair* (u_h^i, r_h^i) *be prescribed by* (5.14)–(5.17)*. Let* $\boldsymbol{\sigma}_{h,\mathrm{disc}}^i$ *be given by Definition 5.1 when* $\vartheta = 0$ *or by Definition 5.7 for all* $\vartheta \in \{-1, 0, 1\}$*. Then Assumption 4.11 is satisfied.*

Finally, the potential reconstructions s_h^i can be obtained by either Definition 5.5, or by Definition 5.6.

5.4 Finite volumes

This section presents a general finite volume approximation for problem (3.2). Finite volumes seek, cf. [21], the discrete pressure $\bar{u}_h \in \mathbb{P}_0(\mathcal{T}_h)$ associated with $\mathsf{U}_h := (\bar{u}_h|_K)_{K\in\mathcal{T}_h}$ such that

$$\sum_{e\in\mathcal{E}_K} \Psi_{K,e}(\mathsf{U}_h) = (f,1)_K \quad \forall K \in \mathcal{T}_h, \tag{5.21}$$

where $\Psi_{K,e}(\mathsf{U}_h)$ is any conservative finite volume flux function for each face e of an element $K \in \mathcal{T}_h$, defined from the discrete pressures U_h. The algebraic residual equation simply reads [18, 25] as

$$\mathsf{R}_K^i := (f,1)_K - \sum_{e\in\mathcal{E}_K} \Psi_{K,e}(\mathsf{U}_h^i) \quad \forall K \in \mathcal{T}_h. \tag{5.22}$$

The piecewise constant residual function $r_h^i \in \mathbb{P}_0(\mathcal{T}_h)$ is then defined by

$$r_h^i|_K := \mathsf{R}_K^i/|K|. \tag{5.23}$$

Following [18, 25] and the references therein, we trivially set:

Definition 5.9 (Flux reconstruction by direct prescription)**.** *Define* $\boldsymbol{\sigma}_{h,\mathrm{dis}}^i \in \boldsymbol{RTN}_0(\Omega)$ *by*

$$(\boldsymbol{\sigma}_{h,\mathrm{dis}}^i\cdot\boldsymbol{n}_e,1)_e := \Psi_{K,e}(\mathsf{U}_h^i) \quad \forall e \in \mathcal{E}_K, \quad \forall K \in \mathcal{T}_h. \tag{5.24}$$

We then immediately have:

Lemma 5.10 (Assumption 4.11)**.** *Let the pair* $(\bar{u}_h^i, r_h^i)$ *be given by* (5.21)–(5.23) *and* $\boldsymbol{\sigma}_{h,\mathrm{disc}}^i$ *by Definition 5.9. Then Assumption 4.11 holds with* $p = 0$.

The approximate finite volume solution $\bar{u}_h^i \in \mathbb{P}_0(\mathcal{T}_h)$ is only piecewise constant. Therefore, to compute the a posteriori estimate (4.16), we first construct a postprocessed approximation $u_h^i \in \mathbb{P}_2(\mathcal{T}_h)$ that is defined elementwise following [18, 25] and the references therein as

$$-\underline{\boldsymbol{K}}\nabla u_h^i|_K\cdot\boldsymbol{n}_e = \frac{\Psi_{K,e}(\mathsf{U}_h^i)}{|e|} \quad \forall e \in \mathcal{E}_K, \quad \forall K \in \mathcal{T}_h,$$
$$\frac{(u_h^i,1)_K}{|K|} = \bar{u}_h^i|_K \quad \forall K \in \mathcal{T}_h.$$

Then, we set $s_h^i := \mathcal{I}_{\mathrm{av}}(u_h^i) \in \mathbb{P}_2(\mathcal{T}_h)$ to obtain the potential reconstruction in the sense of Definition 4.1.

Remark 5.11 (Mixed finite elements)**.** *Application to mixed finite elements is also simply possible following [18, 20].*

6 Numerical experiments

In this Section, we consider the application of the goal-oriented a posteriori error estimates of Theorems 4.8 and 4.13 to a finite volume method of Section 5.4. We also numerically illustrate the difference of the goal estimate of Theorem 4.8 with respect to the simple estimate of Remark 4.7 for the nonconforming finite element method of Section 5.2 and present an example where both lead to unsatisfactory results.

Denote the approximate goal functional by $Q_h^i := Q(u_h^i) + (\underline{\boldsymbol{K}}\nabla s_h^i + \boldsymbol{\sigma}_h^i, \underline{\boldsymbol{K}}^{-1}\tilde{\boldsymbol{\sigma}}_h^{i,\mathrm{m}})$. We realize the estimator (4.16) of Theorem 4.8 as a product of a primal estimator $\eta_h^i := \|\underline{\boldsymbol{K}}\nabla s_h^i + \boldsymbol{\sigma}_h^i\|_{\underline{\boldsymbol{K}}^{-\frac{1}{2}}}$ and a dual estimator $\tilde{\eta}_h^i := \|\underline{\boldsymbol{K}}\nabla \tilde{s}_h^i + \tilde{\boldsymbol{\sigma}}_h^i\|_{\underline{\boldsymbol{K}}^{-\frac{1}{2}}}$. Then the goal estimate (4.16) reads

$$e_h^i := |Q(u) - Q_h^i| \le \frac{\eta_h^i\,\tilde{\eta}_h^i}{2} + \left|\left((\underline{\boldsymbol{K}}\nabla s_h^i + \boldsymbol{\sigma}_h^i)\cdot\boldsymbol{n}, \tilde{u}_{\mathrm{D}}\right)_{\Gamma_{\mathrm{D}}} + Q(s_h^i - u_h^i)\right| =: \eta_{h,\mathrm{goal}}^i.$$

The finite volume method we consider is defined on a possibly nonmatching mesh of general polygonal or polyhedral elements, popular in porous media applications. To cast this setting in the framework of the present paper, we follow [48] and in particular suppose that there exists a virtual simplicial submesh of the polytopal mesh which is matching, shape-regular, and such that any polytopal element is covered by a patch of simplices. For a fast evaluation of the estimators η_h^i and $\tilde{\eta}_h^i$, we proceed as in [48, Theorem 3.12]. Following Theorem 4.13, the error components are then distinguished as

$$\eta_h^i \le \eta_{h,\mathrm{disc}}^i + \eta_{h,\mathrm{alg}}^i \text{ where } \eta_{h,\mathrm{disc}}^i := \|\underline{\boldsymbol{K}}\nabla s_h^i + \boldsymbol{\sigma}_{h,\mathrm{disc}}^i\|_{\underline{\boldsymbol{K}}^{-\frac{1}{2}}} \text{ and } \eta_{h,\mathrm{alg}}^i := \|\boldsymbol{\sigma}_{h,\mathrm{alg}}^i\|_{\underline{\boldsymbol{K}}^{-\frac{1}{2}}}, \tag{6.1a}$$

$$\tilde{\eta}_h^i \le \tilde{\eta}_{h,\mathrm{disc}}^i + \tilde{\eta}_{h,\mathrm{alg}}^i \text{ where } \tilde{\eta}_{h,\mathrm{disc}}^i := \|\underline{\boldsymbol{K}}\nabla \tilde{s}_h^i + \tilde{\boldsymbol{\sigma}}_{h,\mathrm{disc}}^i\|_{\underline{\boldsymbol{K}}^{-\frac{1}{2}}} \text{ and } \tilde{\eta}_{h,\mathrm{alg}}^i := \|\tilde{\boldsymbol{\sigma}}_{h,\mathrm{alg}}^i\|_{\underline{\boldsymbol{K}}^{-\frac{1}{2}}}. \tag{6.1b}$$

Moreover, these estimators are localized as

$$\eta_{h,\mathrm{disc},K}^i := \|\underline{\boldsymbol{K}}\nabla s_h^i + \boldsymbol{\sigma}_{h,\mathrm{disc}}^i\|_{\underline{\boldsymbol{K}}^{-\frac{1}{2}};K}, \qquad \eta_{h,\mathrm{alg},K}^i := \|\boldsymbol{\sigma}_{h,\mathrm{alg}}^i\|_{\underline{\boldsymbol{K}}^{-\frac{1}{2}};K},$$
$$\tilde{\eta}_{h,\mathrm{disc},K}^i := \|\underline{\boldsymbol{K}}\nabla \tilde{s}_h^i + \tilde{\boldsymbol{\sigma}}_{h,\mathrm{disc}}^i\|_{\underline{\boldsymbol{K}}^{-\frac{1}{2}};K}, \qquad \tilde{\eta}_{h,\mathrm{alg},K}^i := \|\tilde{\boldsymbol{\sigma}}_{h,\mathrm{alg}}^i\|_{\underline{\boldsymbol{K}}^{-\frac{1}{2}};K},$$

so that we have $\eta_{h,\bullet}^i = \left\{\sum_{K\in\mathcal{T}_h}(\eta_{h,\bullet,K}^i)^2\right\}^{\frac{1}{2}}$ and $\tilde{\eta}_{h,\bullet}^i = \left\{\sum_{K\in\mathcal{T}_h}(\tilde{\eta}_{h,\bullet,K}^i)^2\right\}^{\frac{1}{2}}$ where $\bullet = \mathrm{disc}, \mathrm{alg}$.

For the numerical examples below, we apply Algorithm 1 which includes mesh adaptation as well as adaptive stopping criteria for both the primal and dual linear algebraic solvers, similarly to [32].

6.1 Regular solution, uniform mesh refinement, and inexact solvers

In this test, we consider a two-dimensional problem from [34] of form (3.1) with $\Omega = (0,1)\times(0,1)$, $\Gamma_{\mathrm{D}} = \partial\Omega$, $u_{\mathrm{D}} = 0$, $\underline{\boldsymbol{K}} = \mathrm{Id}$, and the load term f given such that the (regular) exact solution reads

$$u(x,y) = 10^4 x(1-x)y(1-y)\exp\left(-100\left((x-0.75)^2 + (y-0.75)^2\right)\right). \tag{6.3}$$

Note that f is not piecewise polynomial here; we neglect the data oscillation in the primal problem. The goal functional is chosen as

$$Q(u) = \frac{1}{|\omega|}\int_\omega u\,\mathrm{d}\boldsymbol{x} = (\tilde{f}, u)_\Omega, \qquad \tilde{f} = \frac{\chi_\omega}{|\omega|}, \tag{6.4}$$

where $\omega := \{(x,y)\in\Omega : 1.5 \le x+y \le 1.75\}$. In other words, the goal functional is the mean value of the pressure in the strip ω, where the right-hand side function f, the solution u, and gradient of u exhibit large changes. The exact solution is illustrated in the left part of Figure 1, and the zone of interest ω is highlighted in the right part of Figure 1 by the gray region together with the point $(0.75, 0.75)$ (bullet) where the peak of the solution is situated. Comparing (6.4) with (3.3), we see that $\tilde{u}_{\mathrm{D}} = 0$.

The numerical tests are performed on a sequence of uniformly refined meshes $\mathcal{T}_0, \mathcal{T}_1, \ldots, \mathcal{T}_J$, $J = 4$. We employ the Bi-Conjugated Gradient Stabilization (BiCGStab) [47] iterative matrix

Algorithm 1 Goal-oriented adaptive inexact method

Input: Initial mesh $\mathcal{T}_0$, $J \geq 1$ the maximum number of mesh refinement levels, and two real parameters $\gamma_{\text{alg}}, \theta \in (0,1)$.
Set $j = 0$.
While $(j \leq J)$ do

- **INEXACTLY SOLVE**:
  1. Approximately solve the *primal matrix system* $\mathbb{A}\mathsf{U}_h = \mathsf{F}_h$ as follows:
     (a) Choose an initial vector $\mathsf{U}^0 \in \mathbb{R}^N$. Set $i := 0$.
     (b) Perform $\nu > 0$ steps of a chosen iterative linear solver . This yields an approximation $\mathsf{U}_h^{i+\nu}$ to U_h which satisfies: $\mathbb{A}\mathsf{U}_h^{i+\nu} = \mathsf{F}_h - \mathsf{R}_h^{i+\nu}$.
     (c) Set $i := i + \nu$.
  2. Compute the potential reconstruction and the flux reconstructions as follows:
     (a) Compute u_h^i and r_h^i as described in Section 5.
     (b) Construct the discretization flux reconstruction $\boldsymbol{\sigma}_{h,\text{disc}}^i$ from Definition 5.1 or 5.7 or 5.9 or Remark 5.4 and the algebraic error flux reconstruction $\boldsymbol{\sigma}_{h,\text{alg}}^i$ from Definition 8.1.
     (c) Construct the potential reconstruction s_h^i from either Definition 5.5 or Definition 5.6.
  3. **ESTIMATE**. Compute the discretization and algebraic estimators $\eta_{h,\text{disc}}^i$ and $\eta_{h,\text{alg}}^i$ from (6.1a).
  4. Check the stopping criterion of the primal linear solver in the form:
  $$\eta_{h,\text{alg}}^i \leq \gamma_{\text{alg}}\, \eta_{h,\text{disc}}^i. \tag{6.2a}$$
  If not satisfied, go back to step (1b).
  5. Follow the above steps 1–4 to solve the *dual matrix system* $\mathbb{A}\tilde{\mathsf{U}}_h = \tilde{\mathsf{F}}_h$, with the adaptive stopping criterion
  $$\tilde{\eta}_{h,\text{alg}}^i \leq \gamma_{\text{alg}} \tilde{\eta}_{h,\text{disc}}^i \tag{6.2b}$$
  for the estimators from (6.1b).
- **MARK**. Mark sets for each of the primal and dual problems:
  1. Mark a minimal set for the primal problem $\mathcal{M}_{\text{p}} \subset \mathcal{T}_h$ such that
  $$\theta \max_{K \in \mathcal{T}_h} \eta_{h,\text{disc},K}^i \leq \eta_{h,\text{disc},K'}^i, \quad \forall K' \in \mathcal{M}_{\text{p}}.$$
  2. Mark a minimal set for the dual problem $\mathcal{M}_{\text{d}} \subset \mathcal{T}_h$ such that
  $$\theta \max_{K \in \mathcal{T}_h} \tilde{\eta}_{h,\text{disc},K}^i \leq \tilde{\eta}_{h,\text{disc},K'}^i, \quad \forall K' \in \mathcal{M}_{\text{d}}.$$
  3. Set $\mathcal{M} := \mathcal{M}_{\text{p}} \cup \mathcal{M}_{\text{d}}$ the union of marked sets found for primal and dual marking procedures above.
- **REFINE**. Refine the marked set $\mathcal{M}$ and generate refined mesh $\mathcal{T}_{j+1}$. Set $j := j + 1$.

End While

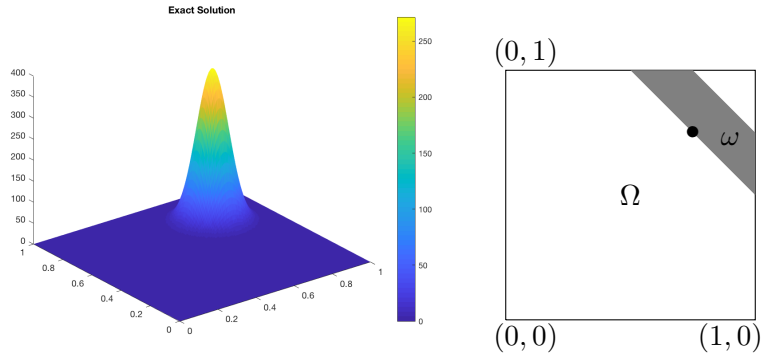

Figure 1: Exact solution (*left*) and the zone of interest (*right*). Section 6.1, goal functional (6.4).

solver with an ILU{0} preconditioner. We first illustrate the **INEXACTLY SOLVE** procedure of Algorithm 1 on the mesh $\mathcal{T}_j$, $j = 2$, with 4×10^4 unknowns. The exact solution as well as the primal and the dual approximate solutions are illustrated in Figure 2, where the color bars represent the distribution of functional values on the xy projected plane. The discretization estimator $\eta^i_{h,\text{disc}}$ (resp. $\tilde{\eta}^i_{h,\text{disc}}$) and the algebraic estimator $\eta^i_{h,\text{alg}}$ (resp. $\tilde{\eta}^i_{h,\text{alg}}$) in function of the iteration counter i are then plotted in the left part (resp. the right part) of Figure 3. In practice, the threshold for the relative algebraic residual is often set as

$$\frac{\|\mathbb{A}\mathsf{U}^i_h - \mathsf{F}_h\|}{\|\mathsf{F}_h\|} \leq 10^{-8} \text{ and } \frac{\|\mathbb{A}\tilde{\mathsf{U}}^i_h - \tilde{\mathsf{F}}_h\|}{\|\tilde{\mathsf{F}}_h\|} \leq 10^{-8}. \tag{6.5}$$

With these stopping criteria, the iterative solvers in the present case need at least 30 iterations, shown in the left and the right part of Figure 3 by the boxes of "std. stop. criteria". It can be observed from Figure 3 that for both the primal and the dual problems, the discretization estimators remain constant after 10 or 15 iterations of the algebraic solver. This is precisely where the adaptive criteria (6.2) (with $\gamma_{\text{alg}} = 0.1$) stop the iterations, enabling to avoid the unnecessary work, see the boxes "adap. stopping criterion" in the left and the right parts of Figure 3.

The convergence histories related to the goal errors e_h (resp. e^i_h) obtained with the inexact ILU{0}-BiCGStab solver with the standard stopping criteria (6.5) and the adaptive stopping criteria (6.2) are plotted in the left part of Figure 4 with respect to the number of unknowns. The effectivity indices defined by the ratio of the estimator to the error $\eta^i_{h,\text{goal}}/e^i_h$ are then shown in the middle part of Figure 4. They lie between 1.6 and 2.6 which we consider excellent. A comparison of the standard stopping criteria (6.5) with the adaptive stopping criteria (6.2) for all the considered meshes $\mathcal{T}_j$, $0 \leq j \leq 4$, is then shown in Figure 4, right. We observe a uniform significant gain with the adaptive stopping criterion.

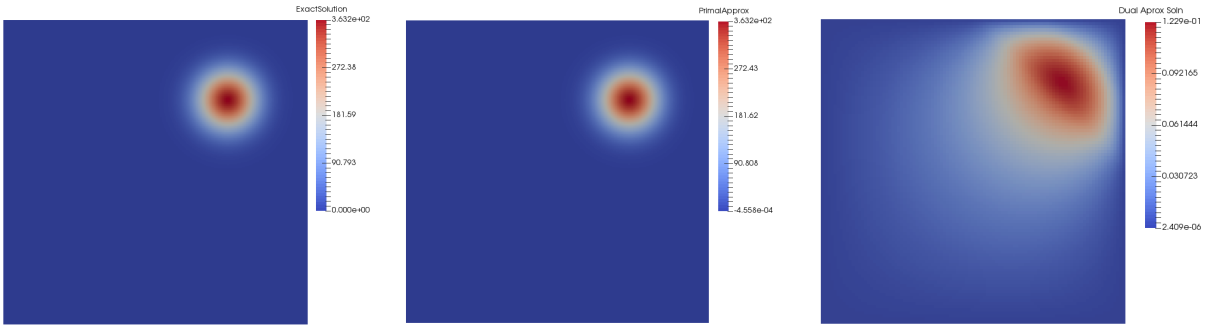

Figure 2: Exact primal solution (*left*), approximate primal solution (*middle*), and approximate dual solution (*right*). Section 6.1, goal functional (6.4).

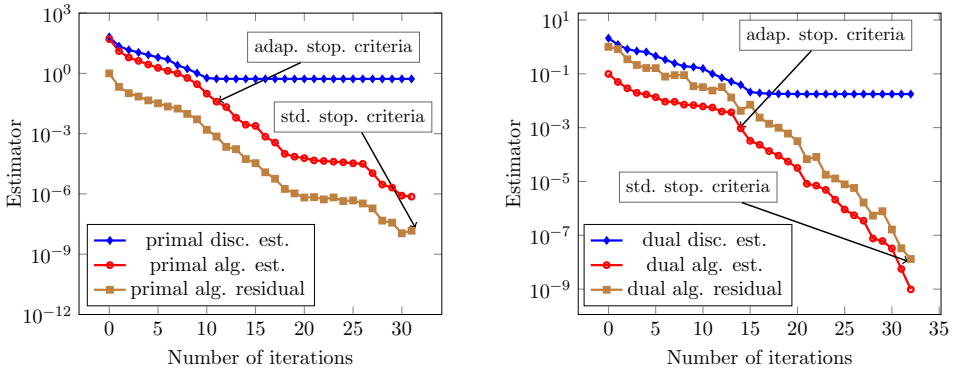

Figure 3: Discretization and algebraic estimators (6.1a)–(6.1b) with standard stopping criteria (6.5) and adaptive stopping criteria (6.2) for the primal (*left*) and the dual problem (*right*) on the mesh $\mathcal{T}_2$ with 4×10^4 unknowns.

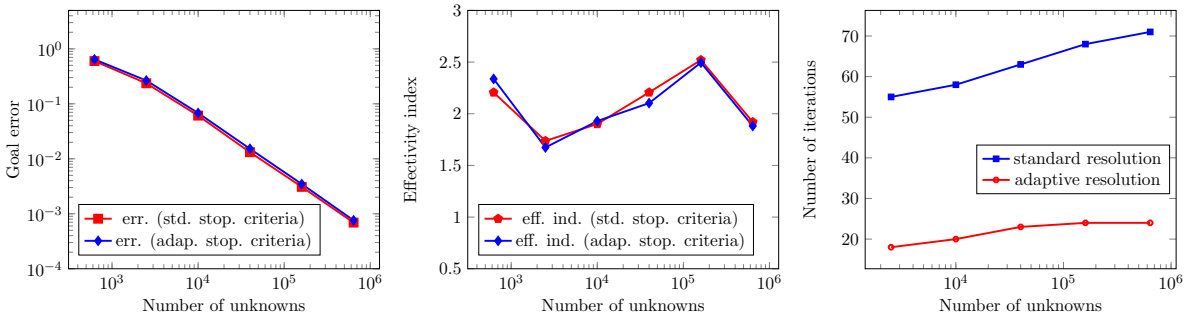

Figure 4: Convergence history of the goal error e_h (resp. e_h^i) on a sequence of uniformly-refined meshes for the ILU{0}-BiCGStab iterative solver with standard (6.5) and adaptive (6.2) stopping criteria with $\gamma_{\text{alg}} = 0.1$ (*left*), and effectivity indices for the goal estimator $\eta_{h,\text{goal}}$ (resp. $\eta_{h,\text{goal}}^i$) (*middle*). Comparison of the number of necessary algebraic solver iterations for the standard (6.5) and adaptive (6.2) stopping criteria on the sequence of meshes $\mathcal{T}_0, \ldots, \mathcal{T}_4$ (*right*). Section 6.1, goal functional (6.4).

6.2 Singular solution, adaptive mesh refinement, and inexact solvers

In this test, we review the standard adaptive mesh refinement procedure SOLVE, ESTIMATE, MARK, and REFINE in the context of goal-oriented a posteriori estimation with our adaptive inexact Algorithm 1, with $\theta = 0.6$. In [7, 24, 33], an exact solver is considered, and the Dörfler marking criterion has been used in the framework of the DWR method. The authors in [33] choose the set with smallest cardinality between $\mathcal{M}_{\mathrm{p}}$ and $\mathcal{M}_{\mathrm{d}}$, whereas the authors [24] use the union of these sets $\mathcal{M}_{\mathrm{p}} \cup \mathcal{M}_{\mathrm{d}}$ as we do in Algorithm 1. Moreover, the authors in [7] choose the marking criteria based on the goal estimator which is represented by sum of the product of primal estimator over an element and dual estimator based on the solution over local patch. In [32], a DWR goal estimator is used to distinguish discretization and algebraic errors. The main emphasis is on the multigrid solver, in extension of the energy error estimates in [5].

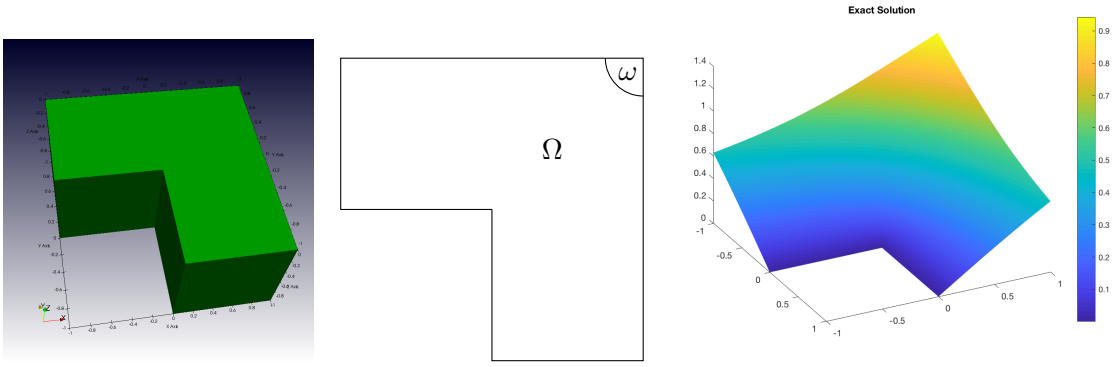

Figure 5: 3D L-shaped domain (*left*), zone of interest on the middle surface (*middle*), and the exact solution (*right*). Section 6.2, goal functional (6.6).

We consider a three-dimensional test case of the form (3.1) with $\underline{\boldsymbol{K}} = \mathrm{Id}$, the right-hand side data function $f = 0$, and the two-dimensional exact solution

$$u(r, \theta, z) = r^{2/3} \sin(2\theta/3)$$

defined on the domain $\Omega = ((-1,1) \times (-1,1) \setminus (-1,0] \times (-1,0]) \times (-1,0)$. The Dirichlet boundary condition on $\Gamma_{\mathrm{D}} = \partial\Omega$ is given by the exact solution as $u_{\mathrm{D}} = u|_{\partial\Omega}$, and we neglect the error due to polynomial approximation of this boundary datum. The zone of interest is considered as $\omega = \{(x, y, z) \in \Omega : (x-1)^2 + (y-1)^2 \leq 0.25^2; z \in (-1, 0)\}$ and the goal functional is defined by

$$Q(u) = \frac{1}{|\omega|} \int_{\omega} u \, \mathrm{d}\boldsymbol{x} = \big(\tilde{f}, u\big)_{\Omega}, \qquad \tilde{f} = \frac{\chi_{\omega}}{|\omega|}. \tag{6.6}$$

The domain Ω, the middle surface, and the exact solution are illustrated in Figure 5. The numerical tests are performed first on a sequence of uniformly refined meshes with standard stopping criteria (6.5) for the inexact ILU{0}-BiCGStab solver and then on a sequence of adaptively refined meshes with adaptive (6.2) stopping criteria with $\gamma_{\mathrm{alg}} = 0.1$ for the inexact ILU{0}-BiCGStab solver, following Algorithm 1. The convergence histories are shown in the left part of Figure 6, and the effectivity indices are plotted in the middle part of this figure. We got effectivity indicies which lie in between 1 and 1.5. Additionally, we observe that adaptive mesh refinement guided by the a posteriori goal estimator leads to rapid error reduction compared to the uniform mesh refinement and a significant gain with the adaptive stopping criterion is obtained in comparison with the standard stopping criteria (6.5).

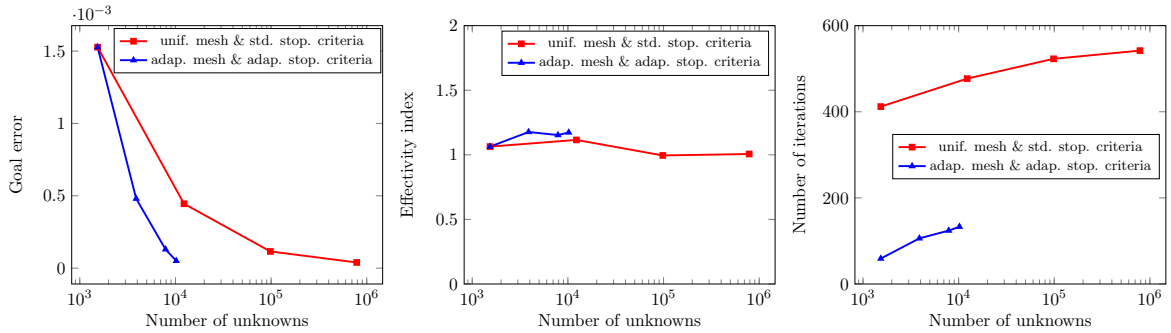

Figure 6: Convergence history of the goal error e_h (resp. e_h^i) (*left*) and the effectivity indices for the goal estimator $\eta_{h,\mathrm{goal}}$ (resp. $\eta_{h,\mathrm{goal}}^i$) (*middle*). Comparison of the number of necessary algebraic solver iterations for the standard (6.5) and adaptive (6.2) stopping criteria (*right*). Section 6.2, goal functional (6.6).

6.3 Heterogeneous media, goal functional given by outflow, uniform mesh refinement, and inexact solvers

In this last test, we consider a heterogeneous porous media with domain $\Omega = (0, 1200) \times (0, 2200)$ partitioned by a grid of 60×220 rectangular cells. The permeability field $\underline{\boldsymbol{K}}$ (scalar times identity) corresponds to the permeability of the layer 85 of the tenth SPE comparative solution project model field [9] and is shown in the left part of Figure 7. We impose a uniform pressure drop from the bottom to the top of the domain with no-flow boundary conditions on the lateral sides. The pressure field on a fine mesh is shown in the right part of Figure 7. In our setting, $\Gamma_{\mathrm{D}} = \{y = 0\} \cup \{y = 2200\}$, $f = 0$, $u_{\mathrm{D}}|_{\{y=0\}} = 1$, $u_{\mathrm{D}}|_{\{y=2200\}} = 0$, and $\sigma_{\mathrm{N}} = 0$. The outflow passing through the surface $\{y = 2200\}$ is defined by

$$Q(u) = -\int_{\{y=2200\}} \underline{\boldsymbol{K}} \nabla u \cdot \boldsymbol{n} \, \mathrm{d}s = -\big(\underline{\boldsymbol{K}} \nabla u \cdot \boldsymbol{n}, \tilde{u}_{\mathrm{D}}\big)_{\Gamma_{\mathrm{D}}}, \qquad \tilde{u}_{\mathrm{D}}|_{\{y=0\}} = 0 \text{ and } \tilde{u}_{\mathrm{D}}|_{\{y=2200\}} = 1. \tag{6.7}$$

Comparing (6.7) with (3.3), we see that $\tilde{f} = 0$. In order to illustrate convergence history, we also consider tests on coarse meshes of 30×110 and 15×55 rectangular cells. We again employ Algorithm 1 with adaptive stopping criteria (6.2) and $\gamma_{\mathrm{alg}} = 10^{-2}$ that we now compare to the "almost exact solve" with the standard algebraic residual criteria (6.5).

In the left part of Figure 8, we show the convergence history of the relative estimator $\eta_{h,\mathrm{goal}}^i / Q_h^i$ with respect to the number of unknowns. In the right part of Figure 8, we plot the number of iterations needed to attain the stopping criteria for the three considered meshes. We observe a significant gain in terms of the number of iterations performed by the ILU{0}-BiCGStab solver with the adaptive stopping criterion.

6.4 Comparison of the estimate of Theorem 4.8 with that of Remark 4.7

In this short section, we consider the nonconforming finite approximation of Section 5.2 with exact solvers and illustrate the difference of the goal estimate (4.16) of Theorem 4.8 with respect to the simple goal estimate (4.14) of Remark 4.7. Let the primal problem be given by

$$\begin{aligned} -\Delta u &= f && \text{in } \Omega, \\ u &= u_{\mathrm{ex}} && \text{on } \partial\Omega, \end{aligned} \tag{6.8}$$

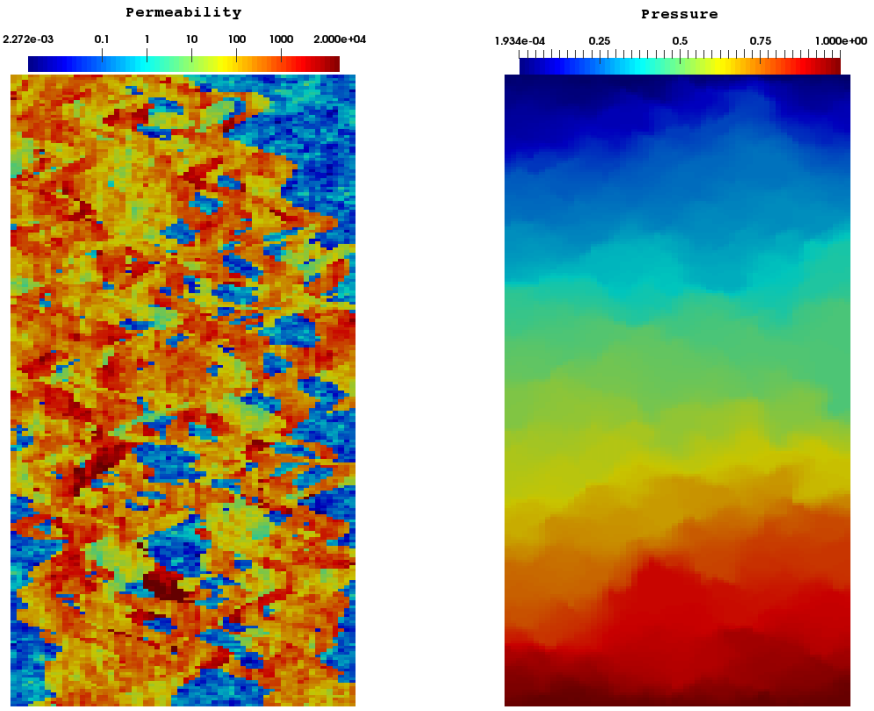

Figure 7: SPE10 permeability (*left*) and pressure field (*right*). Section 6.3.

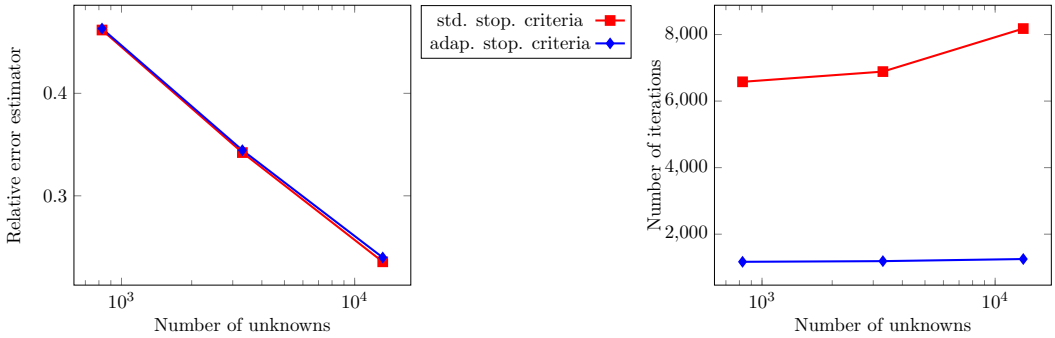

Figure 8: Convergence histories of the relative goal estimators $\eta^i_{h,\mathrm{goal}}/Q^i_h$ with the standard stopping criteria (6.5) and the adaptive stopping criteria (6.2) with $\gamma_{\mathrm{alg}} = 10^{-2}$ (*left*). Comparison of the corresponding number of necessary algebraic solver iterations (*right*). Section 6.3, goal functional (6.7).

where we take $\Omega = (0,1) \times (0,1)$ and $f = 2$ which leads to $u_{\mathrm{ex}}(x,y) = -x^2$. The dual problem is given by

$$\begin{aligned} -\Delta \tilde{u} &= 1 \qquad && \text{in } \Omega, \\ \tilde{u} &= 0 && \text{on } \partial\Omega. \end{aligned} \tag{6.9}$$

In the notation of Section 3, we choose $\underline{\boldsymbol{K}} = \mathrm{Id}$, $\Gamma_{\mathrm{D}} = \partial\Omega$, $\Gamma_{\mathrm{N}} = \emptyset$, $u_{\mathrm{D}} = u_{\mathrm{ex}}|_{\Gamma_{\mathrm{D}}}$, $\tilde{f} = 1$, and $\tilde{u}_{\mathrm{D}} = 0$, which leads to the goal functional $Q(v) = \int_\Omega v \,\mathrm{d}\boldsymbol{x}$, so that $Q(u_{\mathrm{ex}}) = \int_\Omega u_{\mathrm{ex}} \,\mathrm{d}\boldsymbol{x} = -1/3$. Numerical tests are performed on sequence of uniform meshes $\mathcal{T}_j$ with isosceles triangles of size $h_j = \sqrt{2}/2^j, j = 0,1,2,3$.

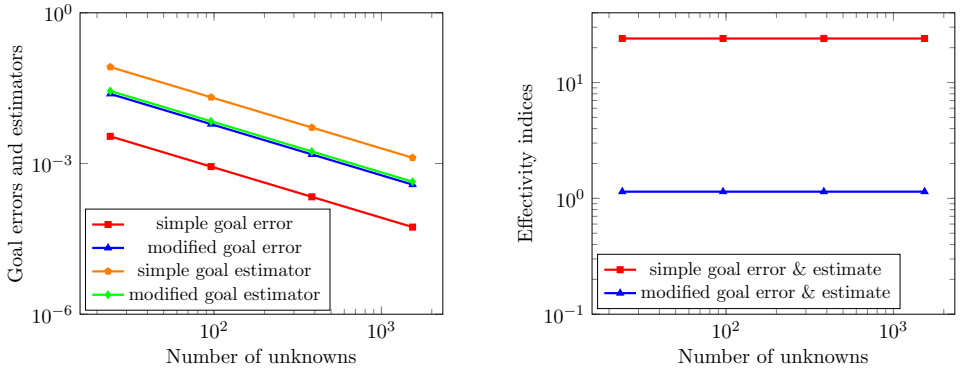

Figure 9: Simple goal error and estimate (4.14) vs. modified goal error and estimate (4.16) (*left*), corresponding effectivity indices (*right*).

The results for the goal error $|Q(u) - Q(u_h)|$ with estimate (4.14) of Remark 4.7 and the modified goal error $|Q(u) - Q(u_h) - \left(\underline{\boldsymbol{K}}\nabla s_h + \boldsymbol{\sigma}_h, \underline{\boldsymbol{K}}^{-1}\tilde{\boldsymbol{\sigma}}_h^{i,\mathrm{m}}\right)|$ with estimate (4.16) of Theorem 4.8 are plotted in the left part of Figure 9. We observe that the estimator of the right-hand side of (4.16) is much smaller than that of the right-hand side of (4.14), which indeed is an important improvement. On the other hand, the goal error on the left-hand side of (4.16) is much bigger than that on the left-hand side of (4.14), so that the "improved" setting of Theorem 4.8 actually deteriorates the goal error. The corresponding effectivity indices are plotted in right part of Figure 9; they are around 24 for the simple goal estimate (4.14) and around 1.14 for the improved goal estimate (4.16). In this respect, i.e., evaluating the quality of the given estimator with respect to the given error, Theorem 4.8 is a real improvement over Remark 4.7.

6.5 A shortcoming of the estimators of Theorem 4.8 and of Remark 4.7

Let us now consider problem (6.8) with $\Omega = (-1,1)\times(-1,1)$ and $f = -2$ in $(-1,0)\times(-1,1)$ and $f = 2$ in $(0,1)\times(-1,1)$. This has a unique solution $u_{\mathrm{ex}}(x,y)$ defined by

$$u_{\mathrm{ex}}(x,y) = \begin{cases} x^2 & \text{in } (-1,0]\times(-1,1), \\ -x^2 & \text{in } (0,1)\times(-1,1). \end{cases} \tag{6.10}$$

We also consider the dual problem (6.9), so that in the notation of Section 3, again $\underline{\boldsymbol{K}} = \mathrm{Id}$, $\Gamma_{\mathrm{D}} = \partial\Omega$, $\Gamma_{\mathrm{N}} = \emptyset$, $u_{\mathrm{D}} = u_{\mathrm{ex}}|_{\Gamma_{\mathrm{D}}}$, $\tilde{f} = 1$, and $\tilde{u}_{\mathrm{D}} = 0$. Numerical tests are performed here on sequence of uniform meshes $\mathcal{T}_j$ which are symmetric across the y-axis, with isosceles triangles of size $h_j = \sqrt{2}/2^j$, $j = 0,1,2,3$; the final mesh $\mathcal{T}_3$ is illustrated in the left part of Figure 10. Recall the goal functional $Q(v) = \int_\Omega v\,\mathrm{d}\boldsymbol{x}$, so that $Q(u_{\mathrm{ex}}) = \int_\Omega u_{\mathrm{ex}}\,\mathrm{d}\boldsymbol{x} = 0$. The computed goal functional on the mesh $\mathcal{T}_3$ then yields $Q(u_h) = -4.900594\text{e-}16$, i.e., is zero up to machine precision. The nonconforming approximation u_h and its potential reconstruction s_h are illustrated, respectively, in the middle and right parts of Figure 10 (on the mesh $\mathcal{T}_1$ for better visibility). The equilibrated fluxes are computed from Remark 5.4. Then, the goal estimates (4.14) and (4.16), respectively, provide on the mesh $\mathcal{T}_3$ the bounds

$$4.900594\text{e-}16 = |Q(u) - Q(u_h)| \le 0.01388889, \tag{6.11a}$$

$$4.351513\text{e-}16 = |Q(u) - Q(u_h) - \left(\underline{\boldsymbol{K}}\nabla s_h + \boldsymbol{\sigma}_h, \underline{\boldsymbol{K}}^{-1}\tilde{\boldsymbol{\sigma}}_h^{i,\mathrm{m}}\right)| \le 0.006944444; \tag{6.11b}$$

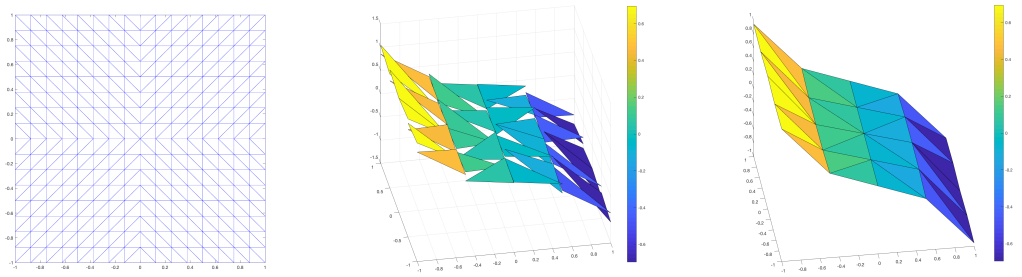

Figure 10: Mesh $\mathcal{T}_3$ symmetric across the y-axis (*left*), the nonconforming approximation u_h on the mesh $\mathcal{T}_1$ (*middle*), and the potential reconstruction s_h on the mesh $\mathcal{T}_1$ (*right*).

here actually all $(\underline{\boldsymbol{K}}\nabla s_h + \boldsymbol{\sigma}_h, \nabla \tilde{s}_h)$, $\big(\underline{\boldsymbol{K}}\nabla s_h + \boldsymbol{\sigma}_h, \underline{\boldsymbol{K}}^{-1}\tilde{\boldsymbol{\sigma}}_h^{\mathrm{m}}\big)$, $((\underline{\boldsymbol{K}}\nabla s_h + \boldsymbol{\sigma}_h)\cdot\boldsymbol{n}, \tilde{u}_{\mathrm{D}})_{\Gamma_{\mathrm{D}}}$, and $Q(s_h)$ are also zero up to machine precision, so that goal errors coincide, and the modified estimator is a half of the simple one (up to machine precision). In this test, both bounds (6.11) extremely overestimate the goal errors, and produce effectivity indices reaching $+\infty$. In particular, the setting of Theorem 4.8 does not bring here any structural improvement over that of Remark 4.7.

7 Conclusion

This paper presents an abstract framework for guaranteed goal-oriented a posteriori error control for various conforming and nonconforming discretizations of the model problem (3.1). It is based on $\boldsymbol{H}(\mathrm{div}, \Omega)$-conforming flux reconstructions and $H^1(\Omega)$-conforming potential reconstructions. The numerical results illustrate that the error in the goal functional (3.3) is estimated very precisely and can be reduced rapidly by applying the adaptive Algorithm 1. Here meshes are refined according to a discretization error estimator and an arbitrary iterative solver is stopped when algebraic and discretization error estimators are in balance. This allows to significantly reduce the number of iterations in the algebraic iterative solver. In particular, the real-life problem of Section 6.3 illustrates an efficient control of the (practically interesting) error in the outflow of fluid through a part of the boundary.

References

[1] M. Ainsworth and R. Rankin, *Fully computable bounds for the error in nonconforming finite element approximations of arbitrary order on triangular elements*, SIAM J. Numer. Anal., 46 (2008), pp. 3207–3232.

[2] ——, *Guaranteed computable bounds on quantities of interest in finite element computations*, Internat. J. Numer. Methods Engrg., 89 (2012), pp. 1605–1634.

[3] W. Bangerth and R. Rannacher, *Adaptive finite element methods for differential equations*, Lectures in Mathematics ETH Zürich, Birkhäuser Verlag, Basel, 2003.

[4] R. Becker, C. Johnson, and R. Rannacher, *Adaptive error control for multigrid finite element methods*, Computing, 55 (1995), pp. 271–288.

[5] R. Becker and R. Rannacher, *An optimal control approach to a posteriori error estimation in finite element methods*, Acta Numer., 10 (2001), pp. 1–102.

[6] D. Braess and J. Schöberl, *Equilibrated residual error estimator for edge elements*, Math. Comp., 77 (2008), pp. 651–672.

[7] M. Bürg and M. Nazarov, *Goal-oriented adaptive finite element methods for elliptic problems revisited*, J. Comput. Appl. Math., 287 (2015), pp. 125–147.

[8] J. H. Chaudhry, E. C. Cyr, K. Liu, T. A. Manteuffel, L. N. Olson, and L. Tang, *Enhancing least-squares finite element methods through a quantity-of-interest*, SIAM J. Numer. Anal., 52 (2014), pp. 3085–3105.

[9] M. Christie and M. Blunt, *Tenth SPE comparative solution project: A comparison of upscaling techniques*, in SPE Reservoir Simulation Symposium, Society of Petroleum Engineers, 2001.

[10] P. Destuynder and B. Métivet, *Explicit error bounds in a conforming finite element method*, Math. Comp., 68 (1999), pp. 1379–1396.

[11] D. A. Di Pietro and A. Ern, *Mathematical aspects of discontinuous Galerkin methods*, vol. 69 of Mathématiques & Applications (Berlin) [Mathematics & Applications], Springer, Heidelberg, 2012.

[12] V. Dolejší, A. Ern, and M. Vohralík, *hp-adaptation driven by polynomial-degree-robust a posteriori error estimates for elliptic problems*, SIAM J. Sci. Comput., 38 (2016), pp. A3220–A3246.

[13] V. Dolejší and F. Roskovec, *Goal-oriented error estimates including algebraic errors in discontinuous Galerkin discretizations of linear boundary value problems*, Appl. Math., 62 (2017), pp. 579–605.

[14] V. Dolejší, I. Šebestová, and M. Vohralík, *Algebraic and discretization error estimation by equilibrated fluxes for discontinuous Galerkin methods on nonmatching grids*, J. Sci. Comput., 64 (2015), pp. 1–34.

[15] V. Dolejší, G. May, A. Rangarajan, and F. Roskovec, *A goal-oriented high-order anisotropic mesh adaptation using discontinuous Galerkin method for linear convection-diffusion-reaction problems*, SIAM J. Sci. Comput., 41 (2019), pp. A1899–A1922.

[16] B. Endtmayer and T. Wick, *A partition-of-unity dual-weighted residual approach for multi-objective goal functional error estimation applied to elliptic problems*, Comput. Methods Appl. Math., 17 (2017), pp. 575–599.

[17] A. Ern, S. Nicaise, and M. Vohralík, *An accurate* $\mathbf{H}(\mathrm{div})$ *flux reconstruction for discontinuous Galerkin approximations of elliptic problems*, C. R. Math. Acad. Sci. Paris, 345 (2007), pp. 709–712.

[18] A. Ern and M. Vohralík, *Adaptive inexact Newton methods with a posteriori stopping criteria for nonlinear diffusion PDEs*, SIAM J. Sci. Comput., 35 (2013), pp. A1761–A1791.

[19] ——, *Four closely related equilibrated flux reconstructions for nonconforming finite elements*, C. R. Math. Acad. Sci. Paris, 351 (2013), pp. 77–80.

[20] ——, *Polynomial-degree-robust a posteriori estimates in a unified setting for conforming, nonconforming, discontinuous Galerkin, and mixed discretizations*, SIAM J. Numer. Anal., 53 (2015), pp. 1058–1081.

[21] R. Eymard, T. Gallouët, and R. Herbin, *Finite volume methods*, in Handbook of Numerical Analysis, Vol. VII, North-Holland, Amsterdam, 2000, pp. 713–1020.

[22] M. B. Giles and E. Süli, *Adjoint methods for PDEs: a posteriori error analysis and postprocessing by duality*, Acta Numer., 11 (2002), pp. 145–236.

[23] R. Hartmann, *Multitarget error estimation and adaptivity in aerodynamic flow simulations*, SIAM J. Sci. Comput., 31 (2008), pp. 708–731.

[24] M. Holst and S. Pollock, *Convergence of goal-oriented adaptive finite element methods for nonsymmetric problems*, Numer. Methods Partial Differential Equations, 32 (2016), pp. 479–509.

[25] P. Jiránek, Z. Strakoš, and M. Vohralík, *A posteriori error estimates including algebraic error and stopping criteria for iterative solvers*, SIAM J. Sci. Comput., 32 (2010), pp. 1567–1590.

[26] O. A. Karakashian and F. Pascal, *A posteriori error estimates for a discontinuous Galerkin approximation of second-order elliptic problems*, SIAM J. Numer. Anal., 41 (2003), pp. 2374–2399.

[27] K. Kergrene, S. Prudhomme, L. Chamoin, and M. Laforest, *A new goal-oriented formulation of the finite element method*, Comput. Methods Appl. Mech. Engrg., 327 (2017), pp. 256–276.

[28] P. Ladevèze, *Strict upper error bounds on computed outputs of interest in computational structural mechanics*, Comput. Mech., 42 (2008), pp. 271–286.

[29] P. Ladevèze and L. Chamoin, *Calculation of strict error bounds for finite element approximations of non-linear pointwise quantities of interest*, Internat. J. Numer. Methods Engrg., 84 (2010), pp. 1638–1664.

[30] P. Ladevèze, F. Pled, and L. Chamoin, *New bounding techniques for goal-oriented error estimation applied to linear problems*, Internat. J. Numer. Methods Engrg., 93 (2013), pp. 1345–1380.

[31] Y. Maday and A. T. Patera, *Numerical analysis of a posteriori finite element bounds for linear functional outputs*, Math. Models Methods Appl. Sci., 10 (2000), pp. 785–799.

[32] D. Meidner, R. Rannacher, and J. Vihharev, *Goal-oriented error control of the iterative solution of finite element equations*, J. Numer. Math., 17 (2009), pp. 143–172.

[33] M. S. Mommer and R. Stevenson, *A goal-oriented adaptive finite element method with convergence rates*, SIAM J. Numer. Anal., 47 (2009), pp. 861–886.

[34] I. Mozolevski and S. Prudhomme, *Goal-oriented error estimation based on equilibrated-flux reconstruction for finite element approximations of elliptic problems*, Comput. Methods Appl. Mech. Engrg., 288 (2015), pp. 127–145.

[35] J.-C. Nédélec, *Mixed finite elements in* $\mathbb{R}^3$, Numer. Math., 35 (1980), pp. 315–341.

[36] J. T. Oden and S. Prudhomme, *Goal-oriented error estimation and adaptivity for the finite element method*, Comput. Math. Appl., 41 (2001), pp. 735–756.

[37] J. Papež, U. Rüde, M. Vohralík, and B. Wohlmuth, *Sharp algebraic and total a posteriori error bounds for h and p finite elements via a multilevel approach*. HAL Preprint 01662944, submitted for publication, 2017.

[38] J. Papež, Z. Strakoš, and M. Vohralík, *Estimating and localizing the algebraic and total numerical errors using flux reconstructions*, Numer. Math., 138 (2018), pp. 681–721.

[39] W. Prager and J. L. Synge, *Approximations in elasticity based on the concept of function space*, Quart. Appl. Math., 5 (1947), pp. 241–269.

[40] S. Prudhomme and J. T. Oden, *On goal-oriented error estimation for elliptic problems: application to the control of pointwise errors*, Comput. Methods Appl. Mech. Engrg., 176 (1999), pp. 313–331. New advances in computational methods (Cachan, 1997).

[41] P.-A. Raviart and J.-M. Thomas, *A mixed finite element method for 2nd order elliptic problems*, in Mathematical aspects of finite element methods (Proc. Conf., Consiglio Naz. delle Ricerche (C.N.R.), Rome, 1975), Springer, Berlin, 1977, pp. 292–315. Lecture Notes in Math., Vol. 606.

[42] V. Rey, P. Gosselet, and C. Rey, *Strict bounding of quantities of interest in computations based on domain decomposition*, Comput. Methods Appl. Mech. Engrg., 287 (2015), pp. 212–228.

[43] ——, *Strict lower bounds with separation of sources of error in non-overlapping domain decomposition methods*, Internat. J. Numer. Methods Engrg., 108 (2016), pp. 1007–1029.

[44] V. Rey, C. Rey, and P. Gosselet, *A strict error bound with separated contributions of the discretization and of the iterative solver in non-overlapping domain decomposition methods*, Comput. Methods Appl. Mech. Engrg., 270 (2014), pp. 293–303.

[45] J. E. Roberts and J.-M. Thomas, *Mixed and hybrid methods*, in Handbook of Numerical Analysis, Vol. II, North-Holland, Amsterdam, 1991, pp. 523–639.

[46] E. H. van Brummelen, S. Zhuk, and G. J. van Zwieten, *Worst-case multi-objective error estimation and adaptivity*, Comput. Methods Appl. Mech. Engrg., 313 (2017), pp. 723–743.

[47] H. A. van der Vorst, *Bi-CGSTAB: a fast and smoothly converging variant of Bi-CG for the solution of nonsymmetric linear systems*, SIAM J. Sci. Statist. Comput., 13 (1992), pp. 631–644.

[48] M. Vohralík and S. Yousef, *A simple a posteriori estimate on general polytopal meshes with applications to complex porous media flows*, Comput. Methods Appl. Mech. Engrg., 331 (2018), pp. 728–760.

8 Appendix: Algebraic error flux reconstruction

Following Papež *et al.* [37], for any given $r_h^i \in \mathbb{P}_p(\mathcal{T}_h)$, an algebraic error flux reconstruction $\boldsymbol{\sigma}_{h,\mathrm{alg}}^i \in \boldsymbol{RTN}_p(\Omega)$ with $\nabla\cdot\boldsymbol{\sigma}_{h,\mathrm{alg}}^i = r_h^i$ and $\boldsymbol{\sigma}_{h,\mathrm{alg}}^i\cdot\boldsymbol{n} = 0$ on Γ_N when $\Gamma_\mathrm{N} \neq \emptyset$ can be constructed by employing an exact coarse solver and a telescoping procedure on a hierarchy of meshes that are

supposed nested but typically non-uniform, issued from Algorithm 1. We describe it below for the sake of completeness.

Let $\{\mathcal{T}_j\}_{j=0}^J$ be a hierarchy of matching partitions with the coarse mesh $\mathcal{T}_0$ and the fine mesh $\mathcal{T}_J := \mathcal{T}_h$. Let $\psi_j^{\boldsymbol{a}} \in \mathbb{P}_1(\mathcal{T}_j) \cap H^1(\Omega)$ stand for the hat basis function associated with vertex $\boldsymbol{a} \in \mathcal{V}_j$ and mesh $\mathcal{T}_j$. For all vertices $\boldsymbol{a} \in \mathcal{V}_j$, let $\mathcal{T}_j^{\boldsymbol{a}}$ be the patch of elements of $\mathcal{T}_j$ that share $\boldsymbol{a}$. Moreover, $\omega_j^{\boldsymbol{a}}$ is the corresponding open subdomain, forming the support of hat basis function $\psi_j^{\boldsymbol{a}}$. Let $V_0 := \mathbb{P}_1(\mathcal{T}_0) \cap H^1_{\mathrm{D}}(\Omega)$ be the conforming space of p-degree polynomials over the coarsest mesh $\mathcal{T}_0$. The coarse level Riesz representer $\rho^i_{0,\mathrm{alg}} \in V_0$ of the algebraic residual r_h^i is found as a solution of

$$(\underline{\boldsymbol{K}} \nabla \rho^i_{0,\mathrm{alg}}, \nabla v_0) = (r_h^i, v_0) \quad \forall v_0 \in V_0. \tag{8.1}$$

Set $\boldsymbol{RTN}_{p,j} := \boldsymbol{RTN}_p(\Omega)$ (with respect to the mesh $\mathcal{T}_j$) and $\mathbb{P}_{p,j} := \mathbb{P}_p(\mathcal{T}_j)$. For a given space X, we use $X(\omega_{j-1}^{\boldsymbol{a}})$ to denote its restriction on the subdomain $\omega_{j-1}^{\boldsymbol{a}} \subset \Omega$ associated with the mesh $\mathcal{T}_{j-1}$. Define the local spaces

$$\begin{aligned}
\boldsymbol{V}_{j,j-1}^{\boldsymbol{a}} &:= \left\{ \boldsymbol{v}_j \in \boldsymbol{RTN}_{p,j}(\omega_{j-1}^{\boldsymbol{a}});\ \boldsymbol{v}_j \cdot \boldsymbol{n}_{\omega_{j-1}^{\boldsymbol{a}}} = 0 \text{ on } \partial\omega_{j-1}^{\boldsymbol{a}} \right\}, \\
Q_{j,j-1}^{\boldsymbol{a}} &:= \left\{ q_j \in \mathbb{P}_{p,j}(\omega_{j-1}^{\boldsymbol{a}});\ (q_j, 1)_{\omega_{j-1}^{\boldsymbol{a}}} = 0 \right\}, \\
&\qquad\qquad \boldsymbol{a} \in \mathcal{V}_{j-1}^{\mathrm{int}} \cup \mathcal{V}_{j-1}^{\mathrm{N}}, \\
\boldsymbol{V}_{j,j-1}^{\boldsymbol{a}} &:= \left\{ \boldsymbol{v}_j \in \boldsymbol{RTN}_{p,j}(\omega_{j-1}^{\boldsymbol{a}});\ \boldsymbol{v}_j \cdot \boldsymbol{n}_{\omega_{j-1}^{\boldsymbol{a}}} = 0 \text{ on } \partial\omega_{j-1}^{\boldsymbol{a}} \setminus \Gamma_{\mathrm{D}} \right\}, \\
Q_{j,j-1}^{\boldsymbol{a}} &:= \mathbb{P}_{p,j}(\omega_{j-1}^{\boldsymbol{a}}), \\
&\qquad\qquad \boldsymbol{a} \in \mathcal{V}_{j-1}^{\mathrm{ext}} \setminus \mathcal{V}_{j-1}^{\mathrm{N}},
\end{aligned}$$

where $\boldsymbol{n}_{\omega_{j-1}^{\boldsymbol{a}}}$ stands for the outward unit normal of the domain $\omega_{j-1}^{\boldsymbol{a}}$. The multilevel algebraic error flux reconstruction reads:

Definition 8.1. *Define the algebraic error flux reconstruction by the telescoping sum over mesh levels*

$$\boldsymbol{\sigma}^i_{h,\mathrm{alg}} := \sum_{j=1}^{J} \sum_{\boldsymbol{a} \in \mathcal{V}_{j-1}} \boldsymbol{\sigma}^{\boldsymbol{a}}_{j,\mathrm{alg}}, \tag{8.2}$$

where the vertex contributions are defined as the solution of the local patch mixed finite element problems: find $(\boldsymbol{\sigma}^{\boldsymbol{a}}_{j,\mathrm{alg}}, \gamma_j^{\boldsymbol{a}}) \in \boldsymbol{V}_{j,j-1}^{\boldsymbol{a}} \times Q_{j,j-1}^{\boldsymbol{a}}$ *such that*

$$(\boldsymbol{\sigma}^{\boldsymbol{a}}_{j,\mathrm{alg}}, \boldsymbol{v}_j)_{\omega_{j-1}^{\boldsymbol{a}}} - (\gamma_j^{\boldsymbol{a}}, \nabla \cdot \boldsymbol{v}_j)_{\omega_{j-1}^{\boldsymbol{a}}} = 0 \qquad \forall \boldsymbol{v}_h \in \boldsymbol{V}_{j,j-1}^{\boldsymbol{a}}, \tag{8.3a}$$

$$(\nabla \cdot \boldsymbol{\sigma}^{\boldsymbol{a}}_{j,\mathrm{alg}}, q_j)_{\omega_{j-1}^{\boldsymbol{a}}} = \big((\mathrm{Id} - \Pi_{j-1})(r_h^i \psi_{j-1}^{\boldsymbol{a}} - \underline{\boldsymbol{K}} \nabla \rho^i_{0,\mathrm{alg}} \cdot \nabla \psi_{j-1}^{\boldsymbol{a}}), q_j\big)_{\omega_{j-1}^{\boldsymbol{a}}} \qquad \forall q_j \in Q_{j,j-1}^{\boldsymbol{a}}, \tag{8.3b}$$

where Π_j *is the* $L^2(\Omega)$*-orthogonal projection onto* $\mathbb{P}_{p,j}$ *except for* $j = 0$ *where* $\Pi_0 := 0$.